NTNU – Trondheim
Norwegian University of
Science and Technology

Mapping Reservoir Changes Using 4D Seismic on the Norne G-segment, Norwegian Sea

Gunnar Aschjem

Petroleum Geoscience and Engineering
Submission date: June 2013
Supervisor: Martin Landrø, IPT

Norwegian University of Science and Technology
Department of Petroleum Engineering and Applied Geophysics

Abstract

Time-lapse seismic can be an important tool for monitoring and planing further development of a producing hydrocarbon field. Use of 4D seismic can make it possible to detect production changes over a relatively large area and match these changes with production data acquired from wells. Undepleted pockets, pressure barriers and injectors out of range can be revealed when interpreting a 4D data set. This can be valuable information when updating reservoir models and when planing new wells an hence, lead to an increased recovery from the field.

The reservoir interval and the oil column in the Norne G-segment are relatively thin. The pore pressure in the segment has been in the range of the bubble point of the hydrocarbons in place. This has led to gas going out of solution and back to oil again as a result of variations in pore pressure. The producer 6608/10-E-4 has extracted the hydrocarbons from the segment while injector 6608/10-F-4 has given pressure support to the producer by injection of water down flank in the water zone. Water has flushed oil as a result of the production of the hydrocarbons and injection of water. All this factors introduces more than one effect that may have affected the seismic response form the field at the same time, making the 4D interpretation in this segment challenging.

In this Master's thesis interpretation of pressure and saturation changes in the Norne G-segment have been performed for the time interval between 2001 and 2006. The work is done by use of amplitude difference data and AVO attributes on the seismic horizon representing top reservoir in addition to time shift analysis on a horizon below the reservoir. Seismic data from 2001, 2003, 2004 and 2006 and well information including paths, production and injection history has been available for this thesis.

Sammendrag

Repetert seismikk kan være et nyttig verktøy for monitorering og videreutvikling av produserende olje- og gassfelt. Ved bruk av 4D seismikk kan det være mulig å detektere produksjonsendringer over et relativt stort område og sammenligne disse resultatene med produksjonsdata hentet ut fra brønner. Udrenerte lommer, trykkbarrierer og dårlig plasserte injeksjonsbrønner kan bli kartlagt ved tolkning av 4D data. Dette kan være verdifull informasjon når man skal oppdatere reservoarmodeller og planslegge nye brønner, informasjon som kan bidra til økt utvinning fra felt.

Reservoarintervallet og oljekolonnen i G-segmentet på Norne feltet er relativt tynt. Poretrykket i segmentet har vært rundt boblepunktet til hydrokarbonene i feltet. Dette har ført til at gass har gått ut av løsning og tilbake til olje som følge av variasjoner i poretrykket. Produksjonsbrønn 6608/10-E-4 har produsert hydrokarbonene i segmentet hjulpet av vanninjeksjon i brønn 6608/10-F-4 som har opprettholdt trykket i segmentet ved å injesere vann i vannsonen i G-segmentet. Vann har erstattet olje i segmentet som et resultat av produksjon av olje og injeksjon av vann. Alle disse faktorene introduserer mer enn en effekt som kan ha påvirket den seismiske responsen fra feltet på en og samme tid, noe som gjør 4D tolkning utfordrende i dette segmentet.

I denne masteravhandlingen er det gjort tolkning av trykk- og mettningsendringer i G-segmentet på Norne feltet for tidsintervallet 2001 til 2006. Arbeidet er utført med bruk av kart over amplitudeforskjeller og forskjeller i AVO attributter på en seismisk horisont som representerer toppen av reservoaret. I tillegg er analyser av tidsskift på en reflektor under reservoaret utført. Seismisk data fra 2001, 2003, 2004 og 2006 samt brønninformasjon har vært tilgjengelig for denne avhandlingen.

Contents

List of Figures

Acknowledgement

This Master's thesis was carried out during the spring semester 2013 at Norwegian University of Science and Technology (NTNU), Department of Petroleum Engineering and Applied Geophysics. This is the result of my work in the subject TPG4930 - Applied Petroleum Geophysics, Master Thesis.

First of all, a huge thank to my supervisor, Professor Martin Landrø, NTNU, for his guidance, help and discussions while working out this project.

I would like to thank Eivind Bøyum from Schlumberger for giving me a one week training course in use of the Petrel software and Brage Vikaune Aftret for helping me with the Hampson-Russell software.

I would also like to thank Statoil, operator of the Norne field, and its license partners, ENI and Petoro, for the release of the Norne data. Further, I aknowledge the Center for Integrated Operations at NTNU for cooperation and coordination of the Norne Cases.

Last, but not least, I would like to thank my fellow students at "Geolabben" for good discussions, company and allot of fun during this semester.

I will also specify that the view expressed in this paper is my personal view and do not necessarily reflect the views of Statoil and the Norne license partners.

Gunnar Aschjem
Trondheim, June 17, 2013

1 Introduction

Several studies have been done to map the fluid front and pressure build up on the Norne field (e.g. Osdal (2004); Ouair et al. (2005); Lygren et al. (2005); Osdal et al. (2006); Arre (2007)). The earlier publications are generally focused on the main field, segment C, D and E (Figure 2), where most of the production is taking place. Fewer draws their attention to the north-eastern segment, the G-segment. This thesis is mainly focused on the G-segment. The attention will mainly be on addressing reservoir changes to interpretations of 4D amplitude differences and AVO differences on top reservoir and time shifts on a reflector below the reservoir interval.

The Norne G-segment is located in the north-eastern region on the Norne field. In contrast to the main field, the G-segment does only contain hydrocarbon in the uppermost interval, the Garn Formation. The thickness of the Garn Formation is only 25-30 meters in this segment (Osdal et al., 2006; NPD, 2013). The reservoir was initially undersaturated, meaning that the pore pressure in the reservoir prior to production was higher than the bubble point of the oil in place. After start of production in June 2000 the pressure in the segment depleted to below bubble point and gas were going out of solution. The only producer in the G-segment, well 6608/10-E-4, were stopped early 2001 due to lack of pressure support. An injector, well 6608/10-F-4, were drilled to give pressure support to the producer. It started injecting water in September 2001. The pressure in the segment rose after start of injection. Producer E-4 resumed production late summer 2002 an stayed active until the water cut became to high and the producer were stopped July 2005 (Statoil, 2006).

All this changes in pressure and saturation gives changes to the seismic response. A good interpretation of the seismic changes can give valuable information about the pressure and saturation state within the field. Results from 4D studies can easily be implemented in reservoir models and give important information when planning new wells. In 2010 the value of the repeated seismic surveys in the Norne area was estimated to US$4.3 billion. A number that gives motivation to better understand this technology.

2 Study site

The Norne field is located in the Norwegian Sea, offshore Norway, approximately 200 km from the Norwegian coastline, Figure 1. The field covers an area of approximately 9 km x 3 km in block 6608/10 and 6508/1 in the Nordland II area on the transition between the Nordland Ridge and the Dønna Terrace. The water depth in the area is approximately 380 meters and the reservoir is located in a horst block at a depth of 2500 - 2700 meters. The reservoir rocks at Norne are sandstones of lower and middle Jurassic age, separated in four main fault blocks, denoted C, D, E and G for convenience reasons (Ouair et al., 2005). Figure 2 shows a top reservoir map with the location of the different segments in the Norne field.

Figure 1: Location of the Norne field

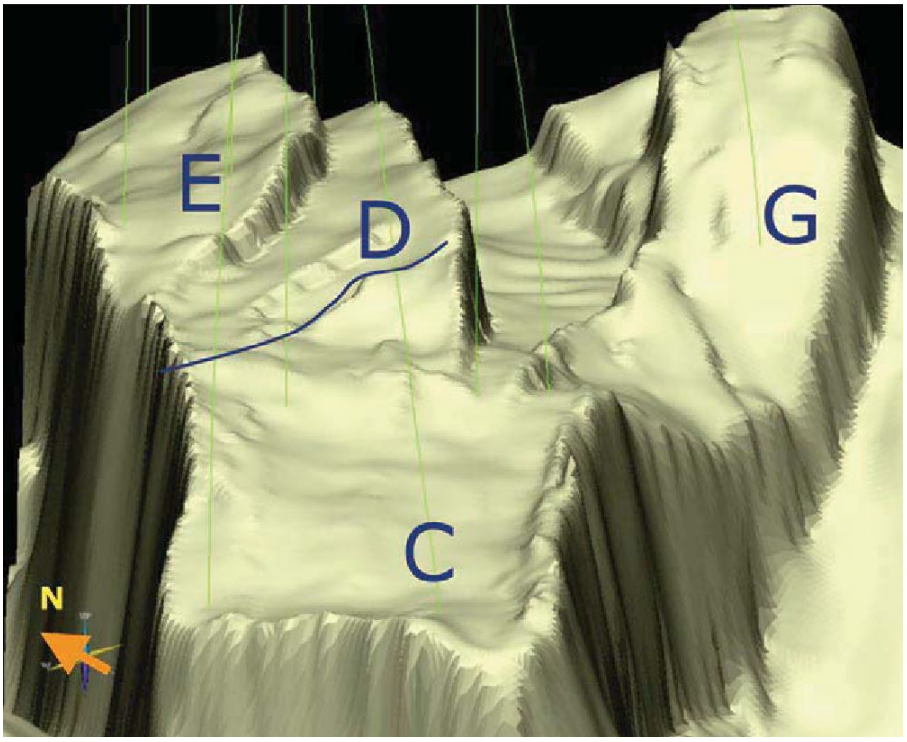

Figure 2: Top reservoir map showing Norne horst block with the four segments. Segment C, D and E builds up the main structure and contain a hydrocarbon column of 135 meter, while segment G only contains oil in the uppermost part of the segment

The field was discovered in December 1991 during the drilling of exploration well 6608/10-2. The well showed a total hydrocarbon column of 135 meter where 110 of them were oil beneath a 25 meters gas cap. To appraise the discovery, exploration well 6608/10-3 was successfully drilled winter 1993. A project to evaluate the fields economic potential and a Plan for Development and Operation (PDO) were worked out on the base of the result from the two exploration wells. In 1994 exploration well 6608/10-4 proved a small oil accumulation in a segment slightly east of the Norne main structure, this was the discovery of the Norne G-segment (Gjerstad et al., 1995).

The licence partners at the field are Statoil Petroleum AS as the operator with a licence share of 39,1% together with Petoro AS (54%) and Eni Norge AS (6,9%).

The Norne field is being developed by a floating production and storage vessel (FPSO) tied to seven subsea templates. The wellstream is carried up to the production vessel in flexible risers. The oil is stored in on board tanks and later loaded onto tankers for export, while gas is being precessed on board and exported through the Åsgård Transport pipeline to the Norwegian mainland at Kårstø (NPD, 2013).

The recovery strategy on the field is to produce the oil with water injection as drive

mechanism. In the beginning of the production gas were injected to give pressure support to the field, but in 2005 all gas injections were cased and export of all gas is now being done. Various measures have been done and considered done to improve the recovery in the field. Time-lapse seismic, or 4D seismic, in combination with pressure data from the field has been used as an important tools to match the production history to the reservoir simulations. New reservoir models have been made on the basis of the 4D results and well positions of planned wells have been changed after updating the models. In 2010 the value of the repeated seismic surveys at Norne was estimated to US$4.3 billion if the surrounding Stær and Svale fields are included (Osdal and Alsos, 2010). Several light well interventions and new production wells are planned this year to maintain the production on the field (NPD, 2013).

The production of oil and gas on Norne peaked in 2001 with a net production of 12,6 million Sm^3 oil equivalents per year. Since then the yearly production has slightly decreased to a level of 0,94 million Sm^3 oil equivalents in 2012. The Norwegian Petroleum Directorate (NPD) reserve estimates from December 2012 estimates the remaining oil equivalents to be 10,72 million Sm^3 of the 105,84 million Sm^3 originally in place (NPD, 2013). Figure 3 shows the yearly net production of oil equivalents from the start-up in 1997 to 2012. In May 2013 the field is producing oil in 17 wells helped by 8 water injectors.

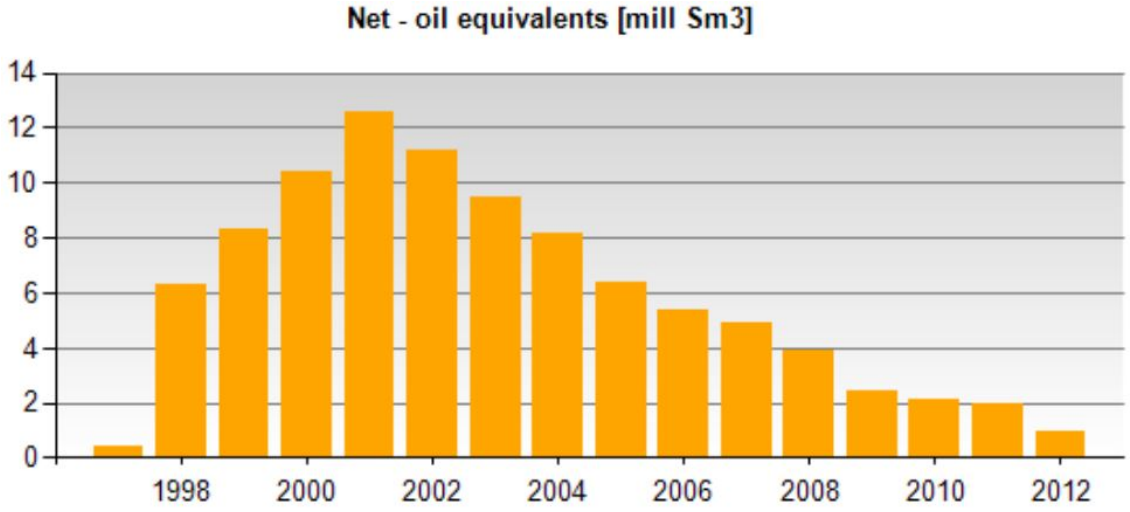

Figure 3: Yearly net production of oil equivalents

2.1 Geologic setting

2.1.1 Structural geology

The Norne field is located in the Nordland II area on the Norwegian Continental Shelf. More precisely in the Revefallet Fault Complex on the transition between the Nordland Ridge and the Dønna Terrace, see Figure 4. The Nordland area has been exposed to two mayor episodes of rifting. One in Permian age and the later one in Late Jurassic to Early Cretaceous age (Statoil, 1994).

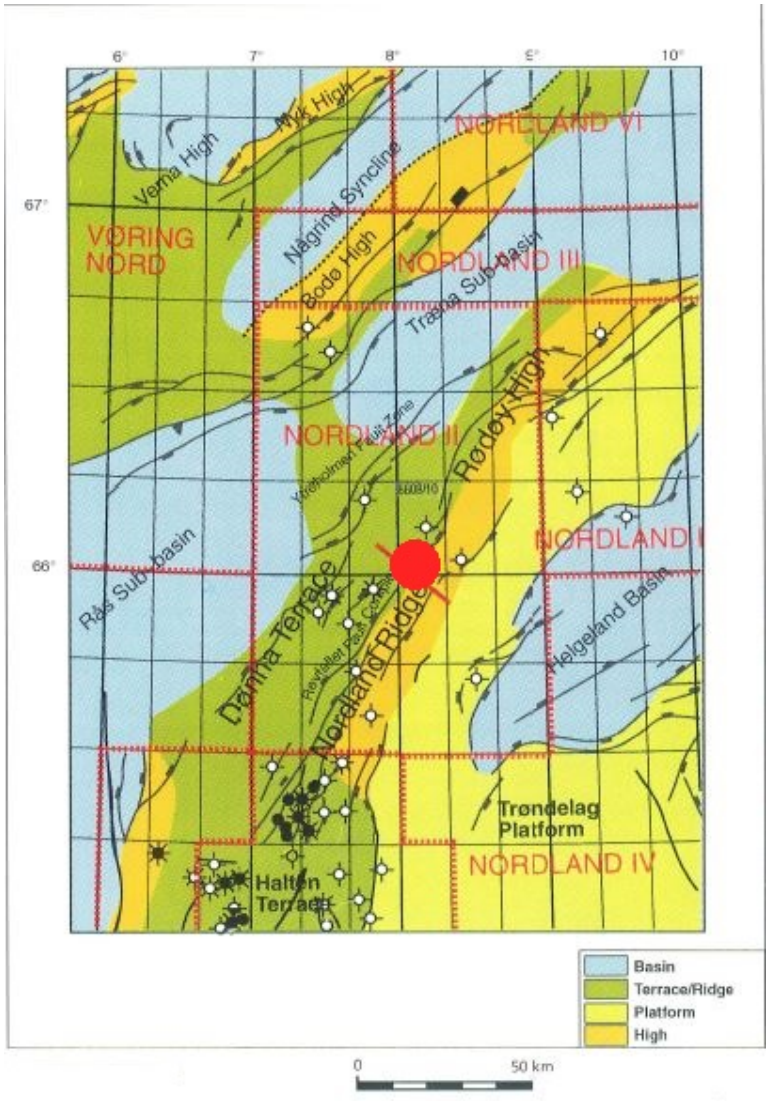

Figure 4: Regional structural setting around the Norne field. From Statoil (1994)

Characteristics of the first rifting period is planar basement-involved normal fault trending in NNE to SSW direction leaving back a block-faulted terrain in the deeper sediments. After the rifting a quite period is registered in late Early Triassic before a period with small fault activity in Mid and Late Triassic. The Late Triassic to

Mid Jurassic was dominated by thermal subsidence, specially in the area to the east of the Nordland Ridge. This resulted in a transgression of the area. Evidences of syn-sedimentation growth faulting originating from this time is found on the Dønna Terrace. The Nordland area does also contain evidences of an unconformity of Toarcian time, probably related to a period of uplift, subaerial exposure and erosion of the underlying sediments. A slight angular discordance of bedding orientation can be found across this unconformity in the north-western part of the Norne Field (Statoil, 1994)

The second rift period can be subdivided into four phases, ranging in age from Late Bathonian to Early Albian time. The rift trend tended to follow the prewious one, NNE to SSE. On the Trøndelag platform footwall uplift occurred, most pronounced along the Nordland Ridge. Structural evaluation in and around the Norne field indicates that the branched Norne horst block is primarily the result of this Late Jurassic to Early Cretaceous rift period. Also erosion in areas with structural highs are connected to this rift period (Statoil, 1994).

After the rift period the Nordland area was subjected to post-rift thermal subsidence. At first it was rapid subsidence to the east of the Nordland Ridge, but after mid Cretaceous the subsidence became most rapid in the area west of the ridge. During Cretaceous the Nordland Ridge remained as a relatively high area and strong erosion was taking place along the ridge (Statoil, 1994). The subsidence continued into the Tertiary except from a slightly doming of the Nordland area as a result of a rearrangement in the spreading-axis in Oligocene (Statoil, 1994)

2.1.2 Stratigraphy and general sedimentology

The reservoir unit in the Norne field is comprised by formations within the Båt- and Fangst Group deposited during Lower and Middle Jurassic age. The reservoir formations within the Båt Group are the Tilje, Tofte and Ror Formations, whereas the Fangst Group is built up by the Ile and Garn Formations. The Ile and Garn Formations is separated by the shaly nonreservoir Not Formation. The base of the reservoir is restricted to the top of the heterolitic Åre formation and the shaly Melke Formation act as a cap rock for the reservoir. The sources for this petroleum system are believed to be the Late Jurassic Spekk Formation and the coal beds within the Åre Formation (Statoil, 1994)

Depositional environment for the Åre formation is associated to be alluvial to delta plain setting before the marginal marine, tidally affected Tilje Formation were de-

posited. Reduced subsidence followed by an uplift in the northern area created a period of less subsidence and subaerial exposure and erosion during the Toarcian time. This caused the Tilje Formation within the field to thin approximately 50 meter to the north. The unconformity marks an distinct change in the quality of the reservoir rocks when it separates the heterolithic sediments of the Åre and Tilje formation from the thicker marine sandstones of the overlying formations (Statoil, 1994)

The Tofte Formation was deposited on top of the unconformity mentioned above and consist of marine, foreshore to offshore sediments of late Toarcian time. The Ror formation were then deposited consisting of sediments deposited on the lower shoreface. The next formation was The Ile Formation that had depositional environment in the shoreface. Within the Ile Formation a sequence boundary can be found, this marks the change from a regressive to a transgressive environment. After the Ile formation the Not Formation was deposited. This is a thin dark grey to black claystone with siltstone lamina deposited under quite marine, probably below wave base, environment. The top of the formation is coarsening upward and the formation is interpreted to contain a flooding surface that marks the transition from a transgressive to a regressive cycle. The Garn Formation was then deposited during the Late Aalenian and the Early Bajocian in a nearshore environment with some tidal influence. The Norne field were again flooded and the sealing Melke Formation were deposited during Late Bajocian to Early Bathonian in an offshore transitional environment. Figure 5 shows a stratigraphical sub-division of the Norne reservoir (Statoil, 1994, 2001b).

Identification of sequence boundaries and flooding surfaces has been performed in the Norne area and correlated between Norne wells 6608/10-2, 6608/10-3 and the surrounding wells 6608/10-1 and 6507/3-1. Lithological boundaries and clear breaks in porosity and permeability has also been correlated throughout the field. This has been used to subdivide the reservoir unit into 17 different zones (Statoil, 1994, 2001b). A cross-section through the reservoir zones can be seen in Figure 6.

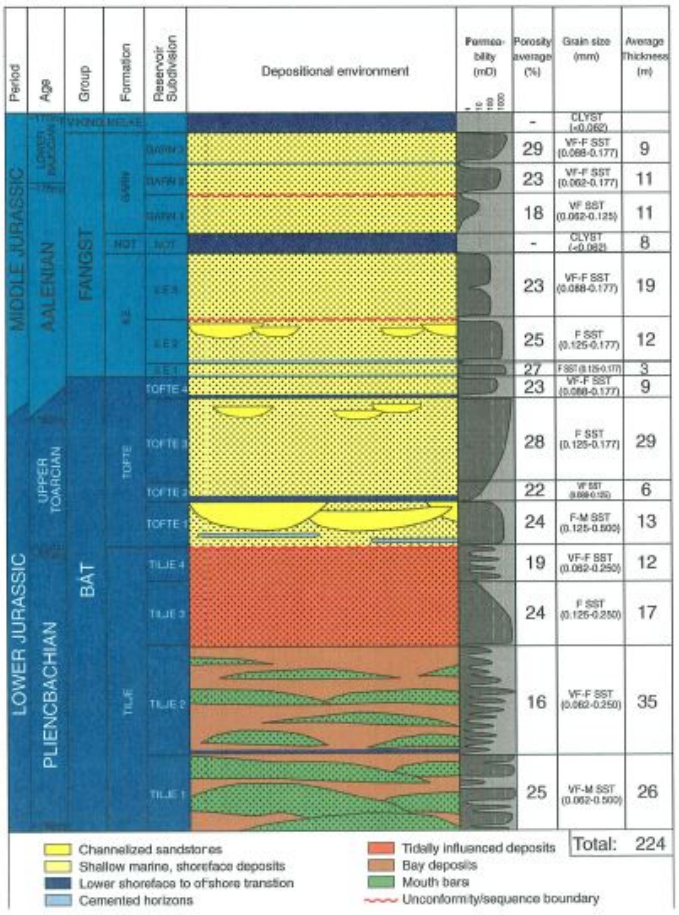

Figure 5: Stratigraphical sub-division of the Norne reservoir. From Statoil (2001b)

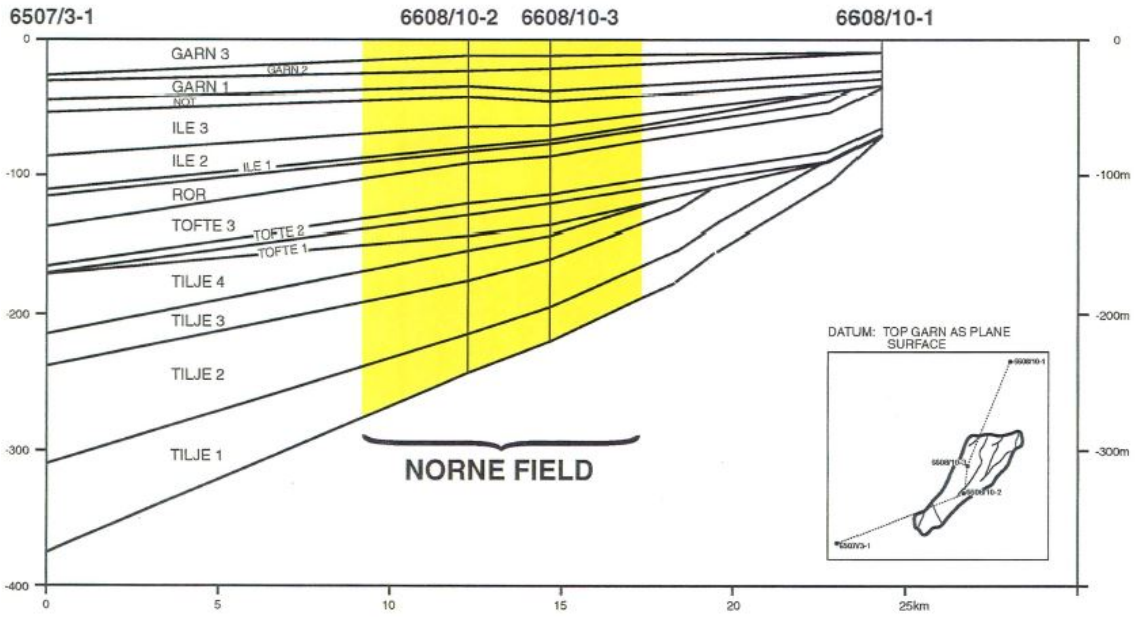

Figure 6: Cross-section through reservoir zone isochores. From Statoil (1994)

3 Dataset

The data available for this thesis are coordinated and administrated by the Center for Integrated Operations at NTNU and consist of seismic surveys form 2001, 2003, 2004 and 2006, well positions and well logs and production and injection data.

3.1 Seismic

The seismic data available for this thesis consist of near-, midt-, far- and full stack seismic data acquired in 2001, 2003, 2004 and 2006 and in addition 2003-2001, 2004-2001 and 2006-2001 difference cubes. To obtain a good repeatability between the seismic surveys all the vintages were acquired by WesternGeco using their Q-Marine technology and a shot geometry consisting of one single source and 6 steerable streamers with 50 m separation (Osdal and Alsos, 2010). The 2001 survey work as a base for the Q-Marine surveys and all the later vintages has been collected with the goal of repeating the acquisition parameters from 2001. Due to gentle currents int the Norne area the repeatability of the acquisition geometry is high. For the far-offset repetition, more than 60% of the shots in 2003 were closer than 25 meter to the 2001 shots (Osdal et al., 2006).

Undershooting of the Norne FPSO has been performed for all the surveys. This has been done in a two-boat operation with one shooting boat and one Q-Marine streamer boat. The acquisition geometry from 2001 has been repeated as good as possible in the later vintages, but poorer results in the undershoot area are obtained compared to the main area. This can be addressed to the timing difficulties associated with a two-boat operations (Osdal et al., 2006). Another source of non repeatability in the undershoot data is the change of source in the 2004 survey. This implemented more NRMS noise to the difference data even with high focus on source matching in the 4D processing steps (Osdal and Alsos, 2010).

Table Table 1 shows the acquisition parameters for the Q-Marine surveys.

Table 1: The acquisition parameters for the Q-Marine surveys (Modification of WesternGeco (2007))

Company	WesternGeco	**Vessel**	Geco Topaz
Survey date	August/Sept. 2001, June 2003, July 2004, July/August 2006	**Survey type**	3D
Instruments	Triacq 5	**Tape format**	SEG-D
Filter settings	High cut 200 Hz Slope 477 dB/oct Low cut 3 Hz Slope 18 dB/oct		
Record length	6144 ms	**Sample rate**	2 ms
Timing delay	64 ms	**Filter delay**	0 ms
Source array	1 x 5085 cu.in. airgun array, operating at 2000 psi		
Source depth	6 m	**Shotpoint interval**	25 m
Receiver array	6 x 3200 m streamer, 240 groups per streamer		
Cable depth	8 m	**Group interval**	12.5 m (DGF)
Inline offset	122 m		
Source separation	n/a	**Cable separation**	50 m
Configuration	254 trace, 64 fold, 6 lines per boat pass, 25 m line spacing		
Polarity convention	Positive pressure at hydrophone recorded as a negative number		

3.1.1 Seismic processing

To obtain good repeatability between the seismic monitoring surveys at the Norne field on board quality check and processing is being preformed. As soon as a line is shot the geometry of the line is compared to the earlier vintages and data from one of the cables are being processed. The acquired data is being ran through designature and radon demultiple before 4D differences is being compared to the earlier vintages. On the basis of this data, quality control is being performed before a decision of keeping or reshooting the line is taken (Osdal and Alsos, 2010).

In addition to quality control full fast track onboard processed 4D data has been available 5-10 days after the end of acquisition. This gives fast access to the new data and can be important in order to maximize the value of the 4D surveys. In 2003 the well path of a planned well was changed after analysis of the fast track onboard data. The new data showed that the originally planned position of a new production well would hit the water zone. A new well path were given and the new producer were successfully drilled into the oil leg. This small position change is estimated by Statoil to have saved 30-60 rig days (Osdal and Alsos, 2010).

To optimize the processing routine and minimizing processing noise the full processing of all Q-Marine surveys at Norne are going through the same processing sequence at WesternGeco. The pre- and post stack processing flows are summarized in Figure 7 and Figure 8.

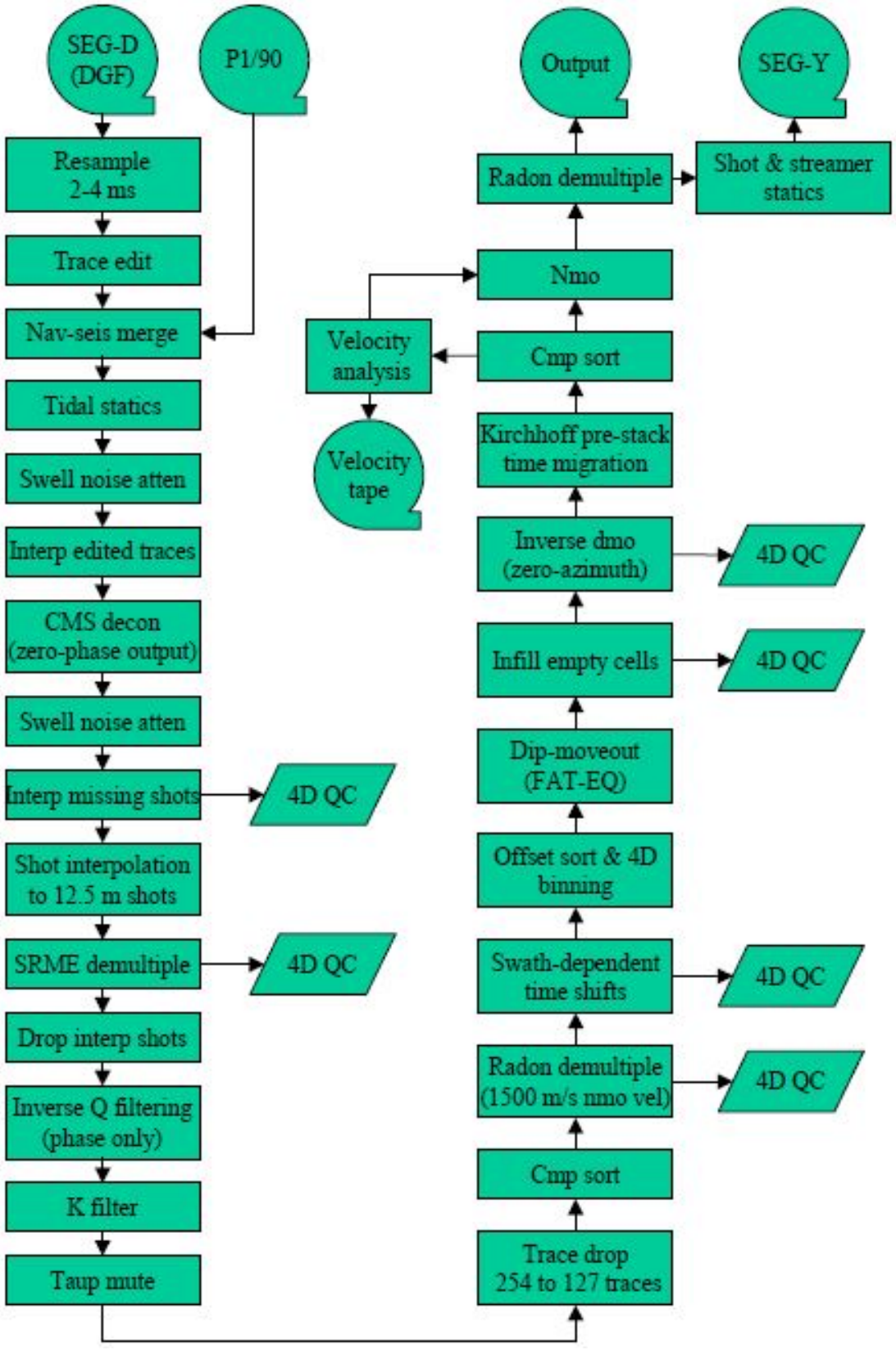

Figure 7: Pre stack processing flow. From Statoil (2006)

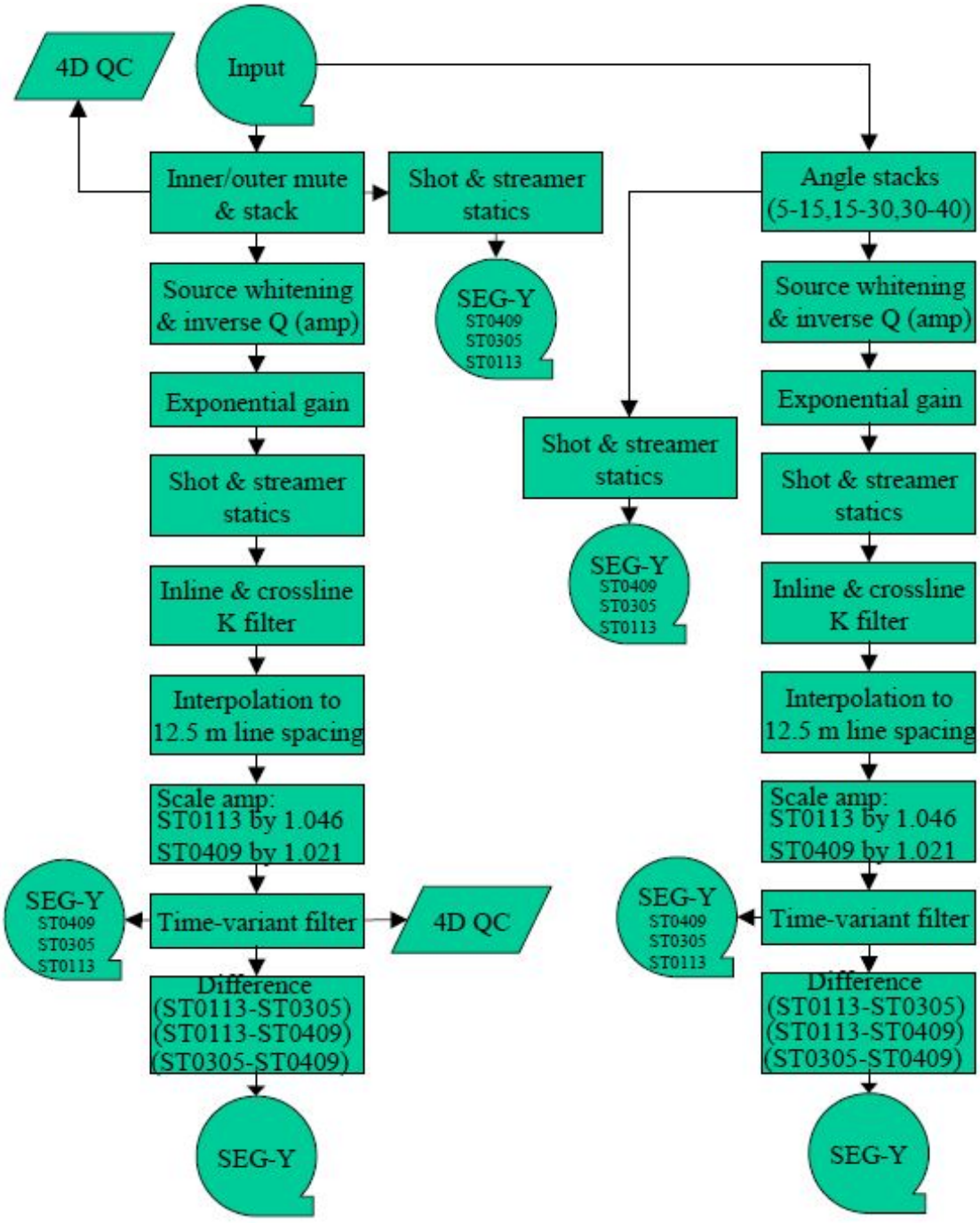

Figure 8: Post stack processing flow. From Statoil (2006)

3.2 Wells

The positions the wells mentioned in this section penetrates the reservoir segments can be seen in Figure 20.

3.2.1 Exploration wells

Exploration well 6608/10-2 was the discovery well for the Norne field. The well was drilled with the primary object to test the hydrocarbon potential of the Middle Jurassic sandstones in the Fangst Group.

The well was spudded on 28th of October 1991 and drilled to a total depth of 3678 meter were it penetrated rocks of the Late Triassic Åre Formation. The well became a success when it in December 1991 encountered oil and gas in the Lower to Middle Jurassic sandstones in the Båt and Fangst Group. After studies of log data and the two FMT tests taken, the well was concluded to be a discovery well containing a 110 meter heigh oil column with an overlying gas cap.

Six cores with a total length of 141.5 meter was recovered from the well and four intervals were perforated and tested for fluid content, temperature and flow rates. The well was permanently abandoned on 29th of January 1992 as an oil and gas discovery (NPD, 2013).

Exploration well 6608/10-4 was drilled to prove hydrocarbon accumulation in the Middle Jurassic sandstones in the north-eastern segment of the Norne field, often referred to as the G-segment, fig 2.

The well was spudded on December 15th, 1993 and drilled to a total depth of 2800 m where it reached rock of the Lower Jurassic Åre Formation. Oil was encountered in the Middle Jurassic sandstones of the Melke Formation and in the Garn Formation. 8 cores in total were cut from the well, spanning from the Cretaceous Nise Formation to the Åre Formation. FMT samples were taken in the Melke, Garn and Ile formation with results of varying quality. The well was plugged and abounded on 7th of March 1994 as an oil and gas discovery (NPD, 2013).

3.2.2 Production and development wells

Well 6608/10-E-4 H was the 17th pilot well on the Norne field. The plan was to test the TVD of the Garn Formation in the G-segment before placing the oil producer

6608/10-E-4 AH (Statoil, 2001a). During the drilling of E-4 H the drilling had to be suspended due to bad weather. The BHA was pulled into the casing. When the drilling team re-entered the well the BHA hit an obstacle that was impossible to bypass. This resulted in the sidetrack 6608/10-E-4 T2 H which was successfully drilled and confirmed the depth of the Garn Formation.

Well 6608/10-E-4 AH was planned to be the 11th oil producer on the Norne field. The well was designed to be a horizontal oil producer located 5-10 meter TVD below the top of the Garn Formation in the north-eastern part of the G-segment. The sidetracking from pilot well 6608/10-E-4 H went after the plan, but problems with a stuck liner running tool during the completion of the well forced the well to be sidetracked to 6608/10-E-4 A T2 H.

Well 6608/10-E-4 A T2 H was successfully drilled and completed with a 600 meter perforated interval in the Garn Formation. The well started production in June 2000, but due to lack of pressure support in the G-segment, the production was stopped between June 2001 until August 2002. In July 2005 the water cut became to high and the production were stopped again. The well resumed production after sidetracking of injector 6608/10-F-4 AH. The well is still an active producer (Statoil, 2001a; Gjerde et al., 2002; Statoil, 2006; NPD, 2013).

Well 6608/10-F-4 H is the 20th development well and the 7th water injector drilled on the Norne Field. The well was placed in the south-western part of the G-segment, downflank of the oil producer E-4 AHT2, Figure 20 (Gjerde et al., 2002).

The objective of the water injector was to give pressure support to the oil producer in the G-segment by injecting water in the water leg downflank of the producer. The well was successfully drilled and started injecting water in September 2001. The pressure in the field rose and producer E-4 AHT2, which had been temporary shut in since March 2001 due to low pressure in the field, could resume production in August 2002. The well were sidetracked into 6608/10-F-4 AH in 2007 to better flush the hydrocarbons to the producer in the G-segment.

Well 6608/10-F-4 AH were sidetracked from injector 6608/10-F-4 to better flush the hydrocarbons to the producer in the G-segment. The well were completed in November 2007 and is still an active water injector.

3.3 Production and injection history

Production and injection history for the field has been available for this thesis. The history contains gas-, oil- and water production rates for the producers in addition to water and gas injection rate for the injectors. Figure 9 shows production and injection history for the producer 6608/10-E-4 and injector 6608/10-F-4.

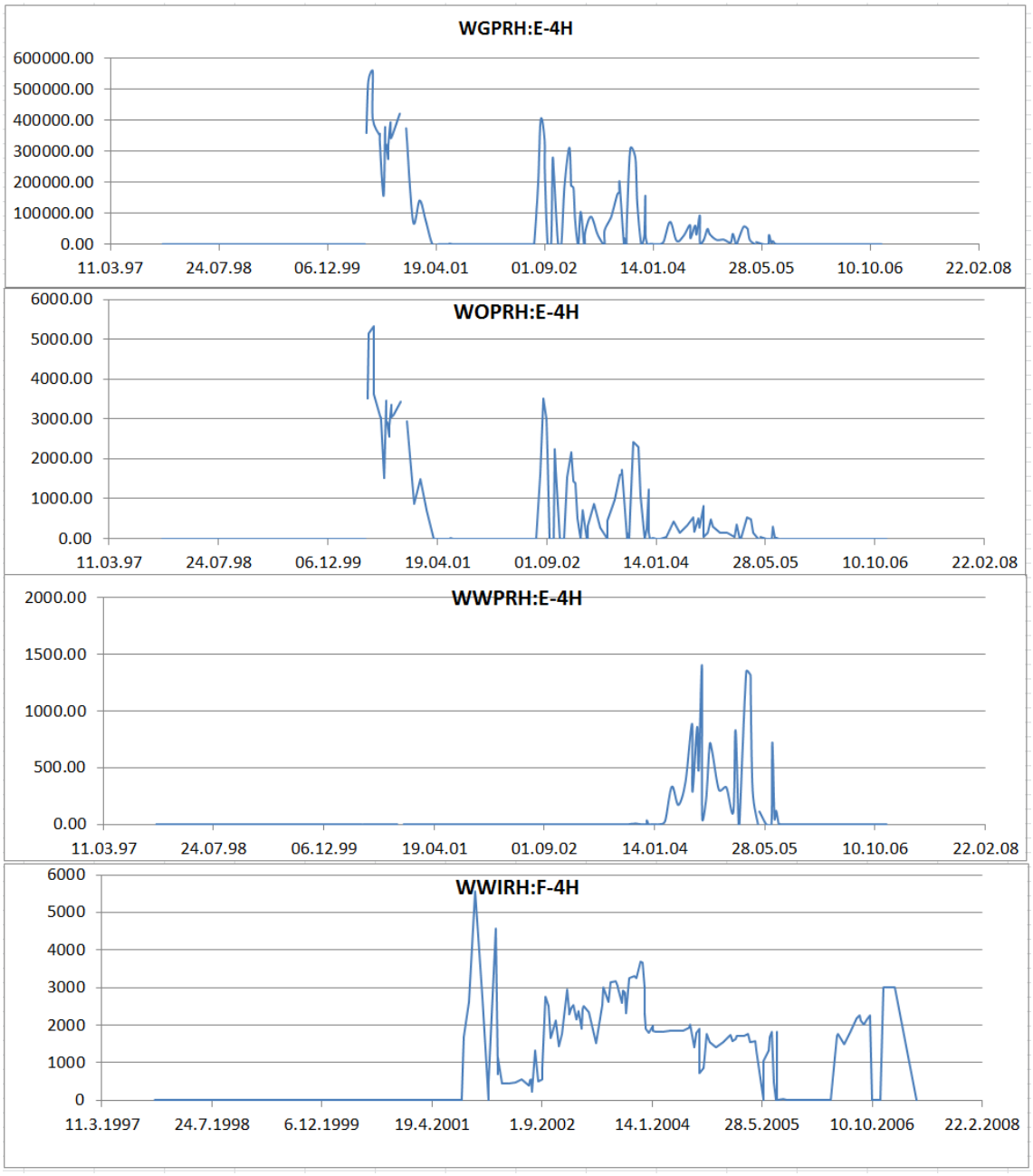

Figure 9: Production history for the producer 6608/10-E-4 and injector 6608/10-F-4. WGPRH: Well Gas Production Rate History, WOPRH: Well Oil Production Rate History, WWPRH: Well Water Production Rate History, WWIRH: Well Water Injection Rate History. All production rates are given in Standard Cubic Meter per Day

4 Theory

4.1 Time-lapse seismology

4D seismology, also known as Time-lapse Seismology is a seismic method growing big the last two decades. As the term 4D describe, it's a seismic survey done in 4 dimensions, three spatial and calendar time as the fourth and last dimension. To confuse a little bit, repeated 2D seismology over time is also named 4D seismology even though it only contains seismic in three dimensions.

It is not clear where and when the first 4D projects started, but Graves and Pulp showed some promising work in the states in 1987 (Greaves and Fulp, 1987). They published a paper where they had done repeated 3D seismology over a heavy oil field and stated that the changes seen on the seismic sections were due to changes in the viscosity of the hydrocarbons as a result of heating the reservoir. They succeed showing some of the strength of 4D seismic, but because of the small size of the reservoir, its shallow depth and the fact that this reservoir was on land, 4D did not get its big break through before Statoil launched their 4D surveys on the Gullfaks field in Northern North Sea, offshore Norway, in 1995. Application of 4D seismology to the Gullfaks field is said to be a great success both technologically and economically (Landrø, 2008).

Today's use of 4D seismic can roughly be divided into three main categories: Monitoring of geohazards (volcano's, rock slides, etc.), monitoring of producing oilfields and monitoring of underground storage of carbon dioxide in saline aquifers. The strength of 4D seismology is that you can observe changes over a relatively large area through time, so application of 4D seismology to a producing oilfield may help you to estimate where and how much hydrocarbons you have extracted from the reservoir and where and how much it is left. It may help you to predict where to find undepleted pockets in complex reservoirs and so on (Landrø, 2011).

4.1.1 Rock physics and its link to 4D seismology

To be able to interpret 4D seismic we need to understand which effects that may affect the seismic response. The link to understand this is use of rock physics. In general there are four main parameters that may change in a producing hydrocarbon reservoir:

- Fluid saturation

- Pore pressure
- Thickness (compaction)
- Temperature

All this parameters changes the seismic response in one way or the other.

Fluid saturation Understanding how changes in fluid saturation affects the seismic response over a reservoir is an important part of 4D monitoring. Relating seismic responses to fluid changes may tell something about the fluid distribution and the movement of fluids within a reservoir. The low frequency Gassmann theory (Gassmann, 1951) is widely used to relate bulk modulus of a saturated rock to its frame, pore and fluid properties, and hence the effect of fluid substitution within a rock unit. Gassmann's equations can be written as:

$$K_{sat} = K_{dry} + \frac{(1 - K_{dry}/K_g)^2}{\phi/K_{fl} + (1-\phi)/K_g - K_{dry}/K_g^2} \tag{1}$$

and the appurtenant result

$$\mu_{sat} = \mu_{eff} \tag{2}$$

where K_{dry} and K_{sat} are the bulk modulus of the dry and saturated bulk unit, K_g and K_{fl} the bulk modulus of the solid grain and fluid, ϕ the porosity and μ_{sat} and μ_{eff} the shear mudulus of the dry and saturated bulk unit. Note that the shear modulus is not affected by the change in fluid.

The density of a rock is also dependent on the fluid:

$$\rho = \phi\rho_{fl} + (1-\phi)\rho_g \tag{3}$$

where ρ is the saturated bulk density, ρ_{fl} the density of the fluid and ρ_g the grain density.

These different rock moduli and densities are related to the P-wave velocity (V_p) and S-wave velocity (V_s) by

$$V_p = \sqrt{\frac{K + \frac{4}{3}\mu}{\rho}} \tag{4}$$

$$V_s = \sqrt{\frac{\mu}{\rho}} \tag{5}$$

Figure 10 shows the change in P- and S-wave velocity as a function of water satura-

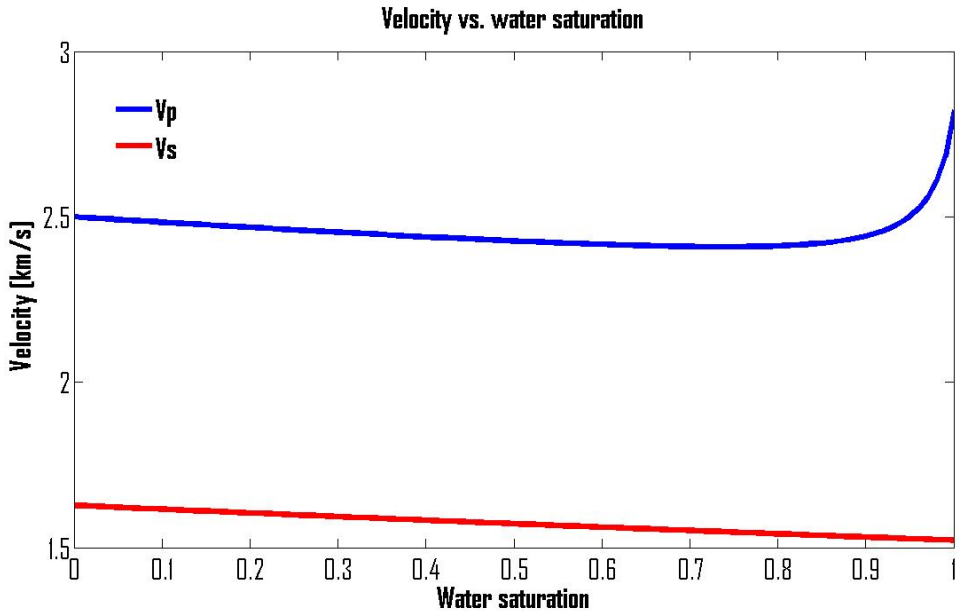

Figure 10: Velocity as a function of water saturation. Note that the P-waves are much more sensitive to the water saturation than the S-waves. Plotted for a formation with 30 % porosity and gas as the other fluid

tion. Note that the P-waves are much more sensitive to the water saturation than the S-waves.

The Gassmann theory is a good indicator of what effects fluid substitution will have on the rock unit, but it has several limitations. The Gassmann equations are only valid for low frequencies where the pore pressure gets time to equilibrate during a seismic period. This is normally not a problem on seismic frequencies <100 Hz, but for log and laboratory measurements where the frequencies normally are >1 kHz, the frequencies falls into the range where Gassmann's equations starts to fail. The main reason why Gassmann's equations fails at high frequencies is that the short seismic periods starts to set up high-frequency wave-induced pressure gradients between pores and cracks, often referred to as the "squirt mechanism" (Mavko and Nur, 1975), that violates the assumption of Gassmann's equations. Tight reservoirs with high degree of microporosity and reservoirs containing fluids with high viscosity can also fail to fulfil the low frequency requirement (Avseth et al., 2005).

Gassmann's equations are also built on the assumption of isotropic rocks with single and homogeneous mineralogy, whose bulk modulus is $K_{mineral}$ in all directions. This is seldom the case in real rocks where almost all are built up of a composition of more than one mineral and are slightly anisotropic. This may lead to either under or over-prediction of the fluid effects calculated using Gassmann's equations (Sava et al., 2000). For the problem with the mixed mineralogy the standard solution is to

use an "average mineral" with properties in between the upper and the lower bound of the mineral mix (Avseth et al., 2005).

Originally Gassmann's equations were designed to do fluid substitution from one pure fluid to another pure fluid, but in field situations it is often a mixture of different fluids within a reservoir. The solution here is normally to use an effective fluid bulk modulus and density (Domenico, 1976; Mavko et al., 2009) and use Gassmann's equations the normal way. If the fluids in the reservoir are mixed at length scale much smaller than a seismic wavelength, Reuss average can be used to calculate the effective fluid bulk modulus ($\bar{K}_{fl}$):

$$\frac{1}{\bar{K}_{fl}} = \sum_i \frac{S_i}{K_{fl_i}} \tag{6}$$

where S_i is the parioal saturation of component i that has a bulk modulus K_{fl_i}. In cases where a producing reservoir has spatial variation in wettability, permeability, shaliness or where structures in the reservoir provoke fingering of pore fluids within the reservoir the fluids can be mixed on a larger scale. We often refer to this state as "patchy saturation" (Avseth et al., 2005) and the effective bulk modulus of the fluids can be calculated using the Voigt average (Mavko et al., 2009):

$$\bar{K}_{fl} = \sum_i S_i K_{fl_i} \tag{7}$$

The effective fluid density ($\bar{\rho}_{fl}$) in both fine scale mixed fluid saturation and patchy fluid saturation is given by:

$$\bar{\rho}_{fl} = \sum_i S_i \rho_{fl_i} \tag{8}$$

where ρ_{fl_i} is the desity of fluid phase i.

Pore pressure In a producing hydrocarbon reservoir the pore pressure in regions of the field may vary through time because of production or injection of fluids. Changing the pore pressure in the reservoir will change the effective stress ($\bar{\sigma}$) in the reservoir as following:

$$\bar{\sigma} = \sigma - \alpha P_p \tag{9}$$

where σ is the hydrostatic confining stress, α the Biot's effective-stress coefficient and P_p the pore pressure. Increased effective pressure will stiffen the rock pack by eliminating some of the pore space, close microcracks and stiffen grain contacts (e.g. Nur and Simmons, 1969; Nur, 1971; Sayers, 1988; Mavko et al., 1995 as cited in Avseth et al. (2005)).

By use of grain pack theories, such as the Hertz-Mindlin's contact theory (Mindlin, 1949), in combination with laboratory measurements one can predict the effect of the pressure changes. Hertz-Mindlin's contact theory estimates the effective bulk (K_{eff}) and shear (μ_{eff}) modulus of a dry, random, identical-sphere packing as:

$$K_{eff} = \left[\frac{C^2(1-\phi)^2\mu_g^2}{18\pi^2(1-\nu)^2}\bar{\sigma}\right]^{\frac{1}{3}} \tag{10}$$

$$\mu_{eff} = \frac{5-4\nu}{5(2-\nu)}\left[\frac{3C^2(1-\phi)^2\mu_g^2}{2\pi^2(1-\nu)^2}\bar{\sigma}\right]^{\frac{1}{3}} \tag{11}$$

where C is the coordination number (the avarage number of contacts per sphere), ϕ the porosity, μ_g the shear modulus of the solid grains and ν Poisson's ratio.

If we assume that the effective pressure in the reservoir at the time of the base survey is P_0 and the effective pressure at monitor survey is P we can insert Equation 10 and Equation 11 into Equation 4 and Equation 5 and find that the relative P- and S-wave velocity versus effective pressure is given as:

$$\frac{V_p}{V_{p_0}} = \left(\frac{P}{P_0}\right)^{\frac{1}{6}} \tag{12}$$

$$\frac{V_s}{V_{s_0}} = \left(\frac{P}{P_0}\right)^{\frac{1}{6}} \tag{13}$$

The relation between effective pressure and P-wave velocity is shown in figure Figure 11.

Generally when comparing theoretically modelled curves like the one seen in Figure 11 to ultrasonic core measurements the slope of the measured curves is lower than the theoretical curve. The reason for this may be more than one: Firstly, the coring process may introduce microcraks or other core damages that affects the stiffness of the rock, the ultrasonic measurements suffers from scaling problems, the grain pack models assume perfect, identical spheres, which you'll never find in the real nature, and last, but not least, the fact that the theoretical models does not take cementation into account (Landrø, 2011).

From Figure 11 one can see that the effect of decreasing the effective stress in the reservoir will have higher impact on the P-wave velocity than increasing it meaning that a pore pressure increase will be easier to detect than a pore pressure decrease. This imply that the 4D effects caused by injectors will be more pronounced than the 4D effects caused by producers if the absolute value of the pressure change is

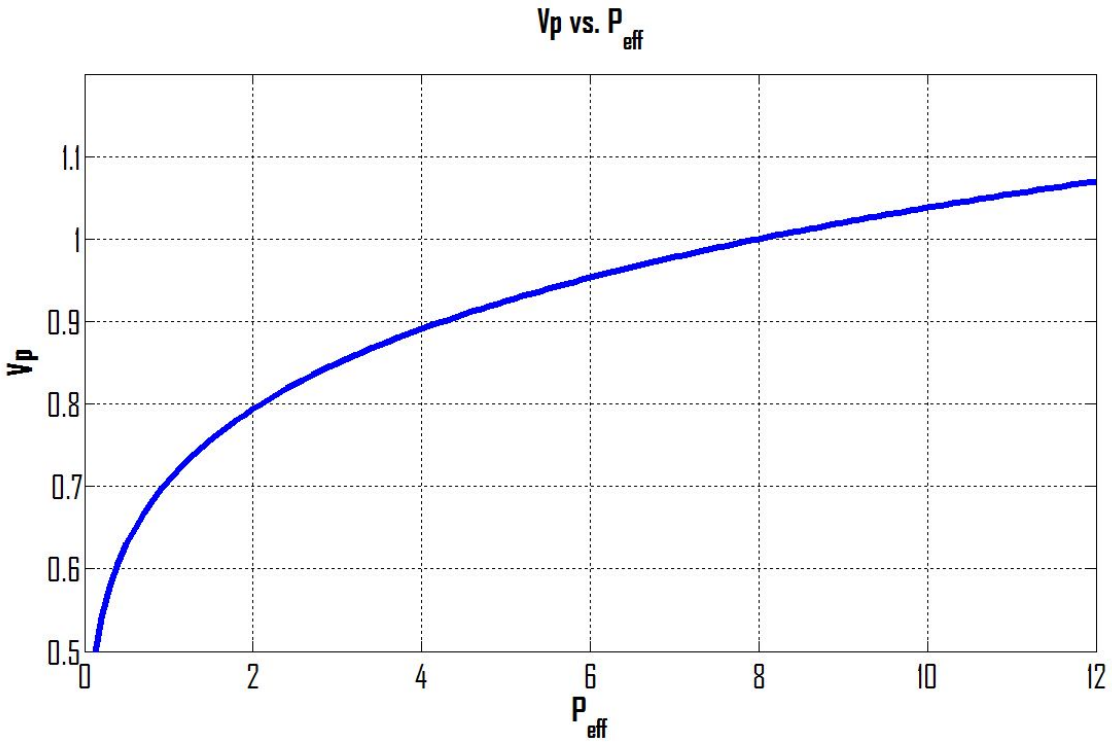

Figure 11: Modelled change in P-wave velocity versus effective pressure using Hertz-Mindlin's contact theory with 8 MPa effective pressure at base survey. We can see that the effect of decreasing the effective pressure has higher impact on the P-wave velocity than increasing it, meaning that a pore pressure increase will be easier to detect than a pore pressure decrease

about the same.

Another important effect of pore pressure changes is the effect of gas going out of solution or back to oil as a result of pore pressure decrease or increase, respectively. Since gas normally has very low bulk modulus compared to oil and brine, this often contribute to a significant 4D effect. The effect the pore pressure has on fluids and the effect pore pressure has on the grain pack works in opposite directions. Higher pore pressure leads to stiffening of the fluids which increases the P-wave velocity. On the other hand, higher pore pressure tends to softening the rock frame and decrease the P-wave velocity. The net effect of this two contradictions is dependent on the fluids and rocks in place and will wary from field to field (Avseth et al., 2005).

Compaction and stretching of formations As mentioned above, pressure depletion as a result of production of the hydrocarbons in a field will increase the effective stress within the reservoir. If the effective stress exceeds the fraction limit of the reservoir rock permanent pore collapse may occur and we will get compaction of the reservoir. Compaction in the reservoir interval will lead to reduced porosity

which generally increases the seismic velocities, which in turn gives negative seismic travel-time shifts between base and monitor surveys. When the reservoir rocks compacts, the over- and under-burden needs to fill in for the compacted space. This leads to a stretching of the over- and under-burden, which in turn gives positive time shifts on the seismic data (Landrø, 2011). Hatchell and Bourne (2005) showed in their work that the accumulative time shift for a compacting reservoir will mainly be positive meaning that the effect of the over-burden stretching is larger than the effect of the compacted reservoir as seen in Figure 12.

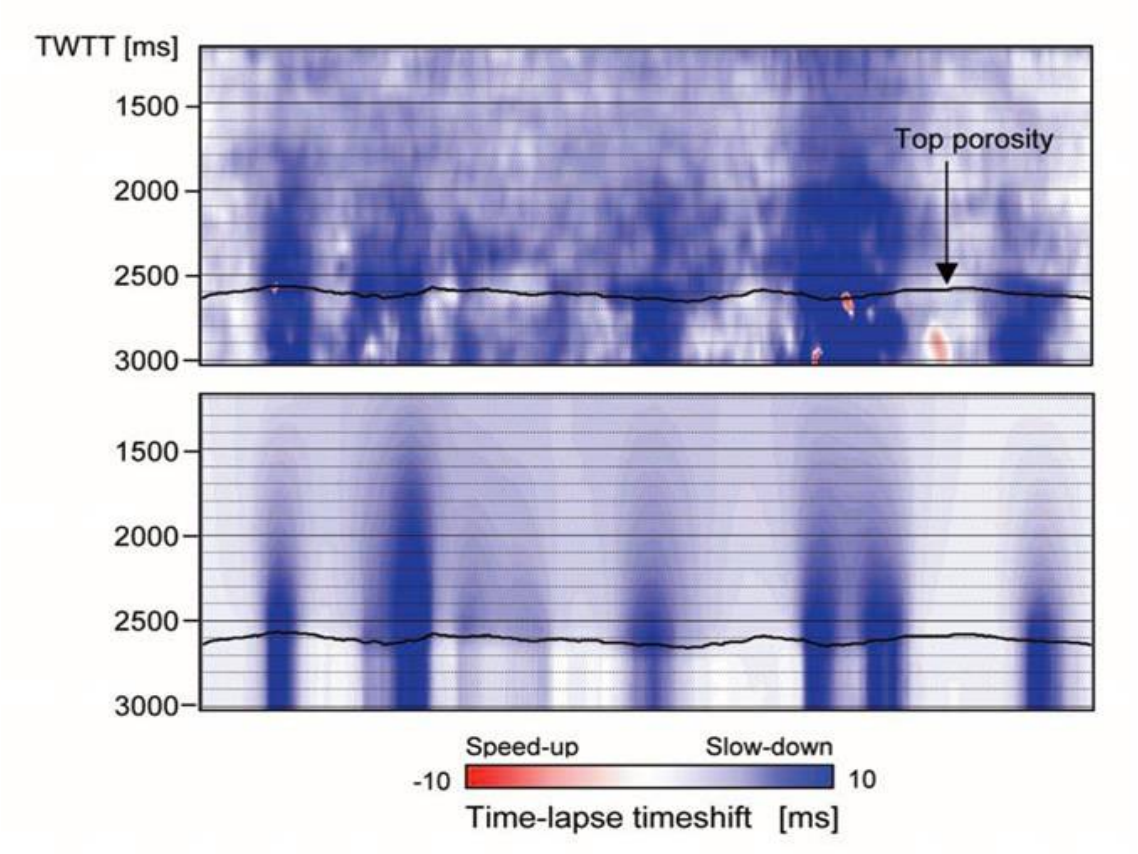

Figure 12: A North Sea chalk reservoir (Norway). Comparison of time-lapse time shifts observed from stacked field data (top) and calculated from an a priori geomechanical model for reservoir depletion (bottom). The depth of the chalk reservoir is about 2400 m with porosities between 35-50 %. Note that the time shifts mainly are positive. From Hatchell and Bourne (2005)

Temperature changes Studies done by Nur et al. (1984) showed that P-wave velocity in oil is strongly dependent of the temperature.This is specially the case for heavy, highly viscous oil. When oil is heated up, the viscosity decrease, which decrease the bulk modulus of the oil and in turn the P-wave velocity. Since water is nearly unaffected by the temperature changes relative to the effect of the heavy oil the temperature changes will be possible to monitor using 4D seimsic. Figure 13 shows the dependence of P-wave velocity on temperature and oil/brine ratio in two oil sands. As mentioned before, Greaves and Fulp (1987) was probably one of the first that did a real 4D survey. Their work is a good example on 4D effects as a result of temperature changes and can be seen in Figure 14.

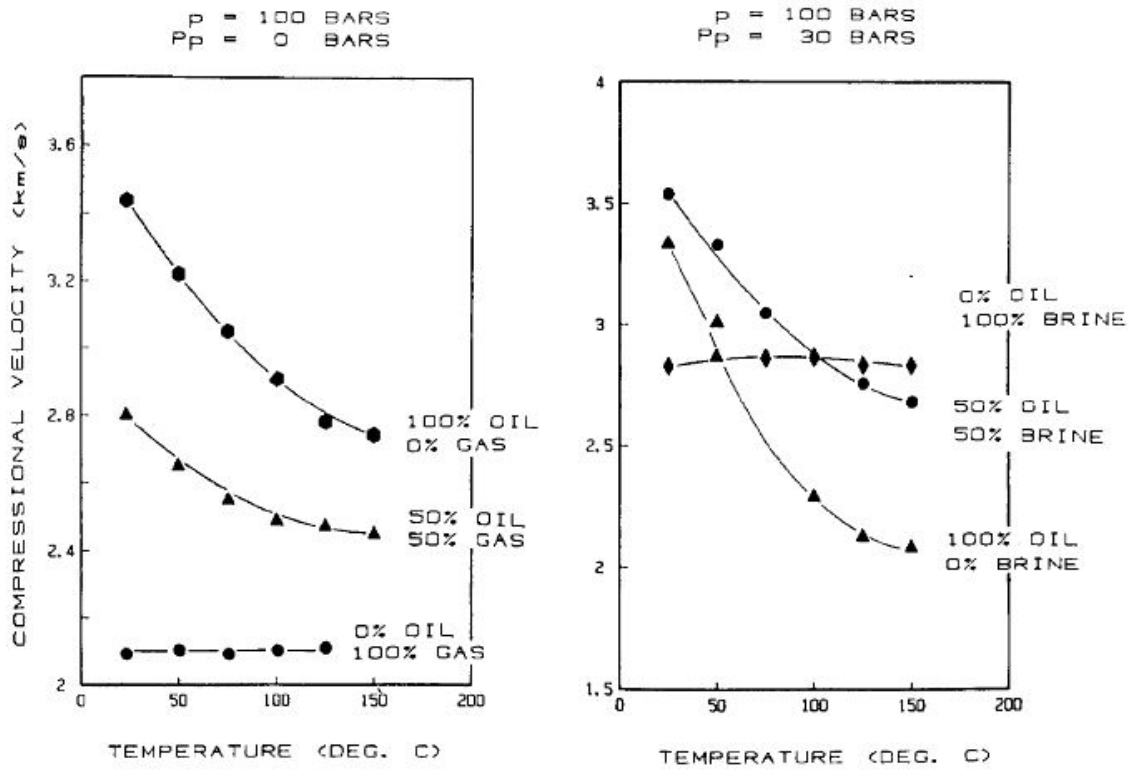

Figure 13: Dependence of P-wave velocity on temperature and oil/brine ratio in oil sands from Kern River, California and Maracaibo, Venezuela. Note that the oil is highly sensitive to temperature changes while the P-wave velocity of the water does not change much at all. From Nur et al. (1984)

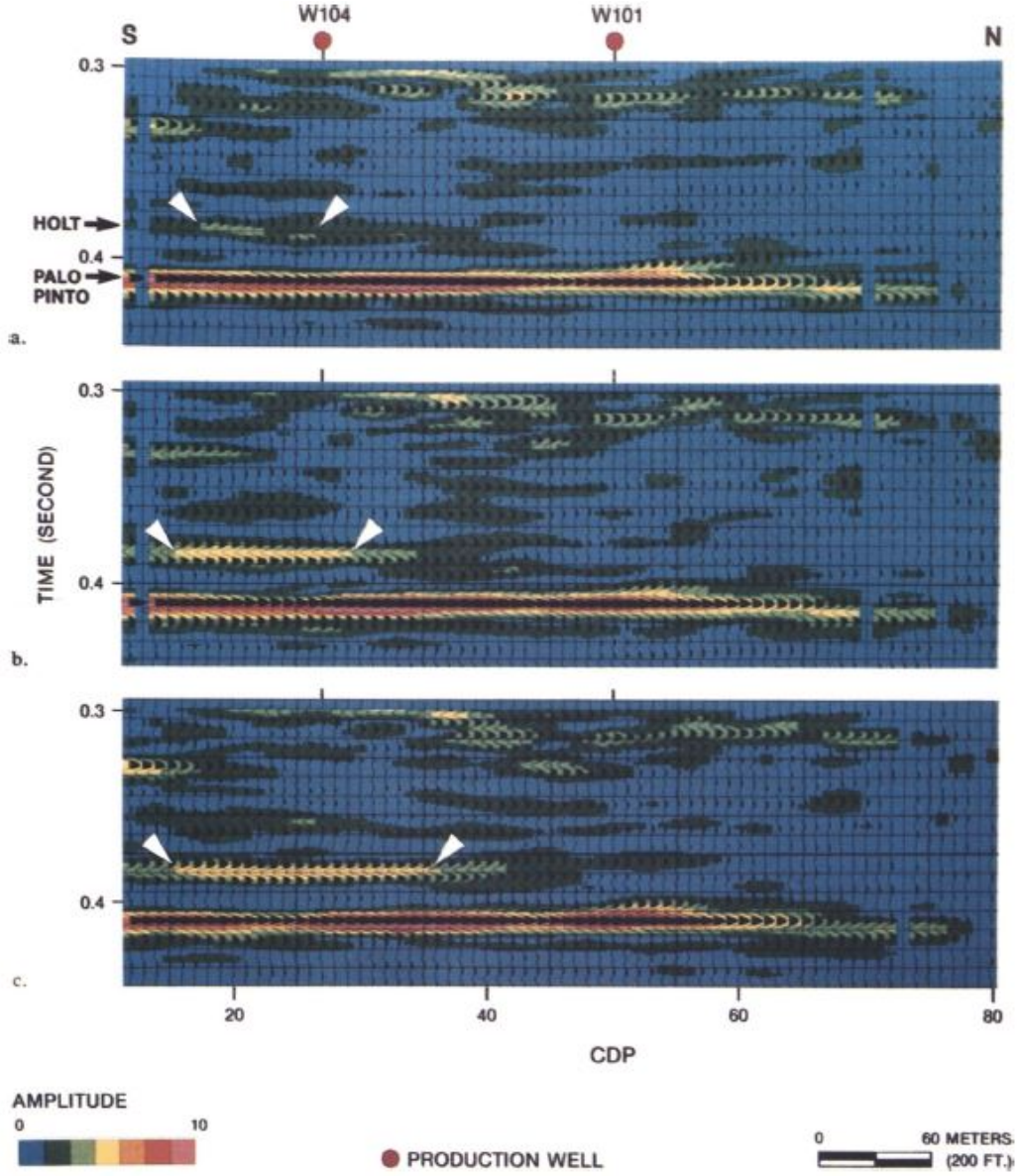

Figure 14: Clear 4D amplitude brightening as a result of heated hydrocarbon reservoir. Note the extent in time as a result of increased temperature distribution in the reservoir. From Greaves and Fulp (1987)

Discriminating between the various effects As described before various effect has an impact on the seismic signals and it can be more than one reason why for example the P-wave velocity in the reservoir has changed. To address the observed seismic 4D change to the changes in the reservoir is often a challenge. A common problem is to discriminate between pore pressure changes and the change in fluid saturation during production. Both a pore pressure decrease and a substitution from oil to water gives normally a higher P-wave velocity in the reservoir, given that the oil is more compressible and lighter than water. One key to distinguish between the different effects is to include more than one measurement of the same reflection point. Saturation changes will mainly affect the P-wave velocity, while the S-wave velocity will almost stay unchanged as Figure 10 shows. Pore pressure changes, on the other hand, will affect both the P- and S-waves as shown in Equation 12 and Equation 13. Information of both P- and S-wave velocity will increase the likelihood of distinguishing between the two cases.

4.1.2 Amplitude versus offset and its link to 4D seismology

In 1919 the famous Zoeppritz equations was published (Zoeppritz, 1919). They showed that the amplitude of a seismic wave is dependent on the incident angle the wave front hits the interface with. This did not become a big thing in the business of hydrocarbon exploration before Ostrander published a break-through paper in *Geophysics* in 1984 (Ostrander, 1984). Ostrander showed that a gas filled sandstone capped by a shale will give a negative variation in amplitude with increasing offset and that this is caused by a reduction of Poisson's ratio in the gas filled sandstone. Shuey confirmed Ostrander's theory the year after by making mathematical approximations of Zoeppritz equations and confirming that Poisson's ratio is the leading elastic constant related to the amplitude variations with variable incidence angle up to an angle of 30° (Shuey, 1985).

After Ostrander and Shuey's publications many approximations to the Zoeppritz equations has been posted through the years. An approximation that is widely used in the exploration industry is the one published by Smith and Gidlow in 1987 (Smith and Gidlow, 1987). This is a slightly simplified version of the approximation derived by Shuey in 1985:

$$R(\theta) = R(0) + Gsin^2\theta + Ftan^2\theta \tag{14}$$

where

$$R(0) = \frac{1}{2}\left(\frac{\Delta V_p}{V_p} + \frac{\Delta \rho}{\rho}\right)$$

and

$$G = -2\frac{{V_s}^2}{{V_p}^2}\left(\frac{\Delta \rho}{\rho} + 2\frac{\Delta V_s}{V_s}\right); \qquad F = \frac{1}{2}\frac{\Delta V_p}{V_p}$$

where θ is the incidence angle. The velocities and densities used in the equations are average values defined as (uses P-waves as example):

$$V_p = \frac{V_{p1} + V_{p2}}{2}$$

$$\Delta V_p = V_{p2} - V_{p1}$$

where V_{p1} is the P-wave velocity for layer 1 and V_{p2} the P-wave velocity for layer 2. Figure 15 shows a schematic drawing of a seismic P-wave hitting an interface with incidence angle θ.

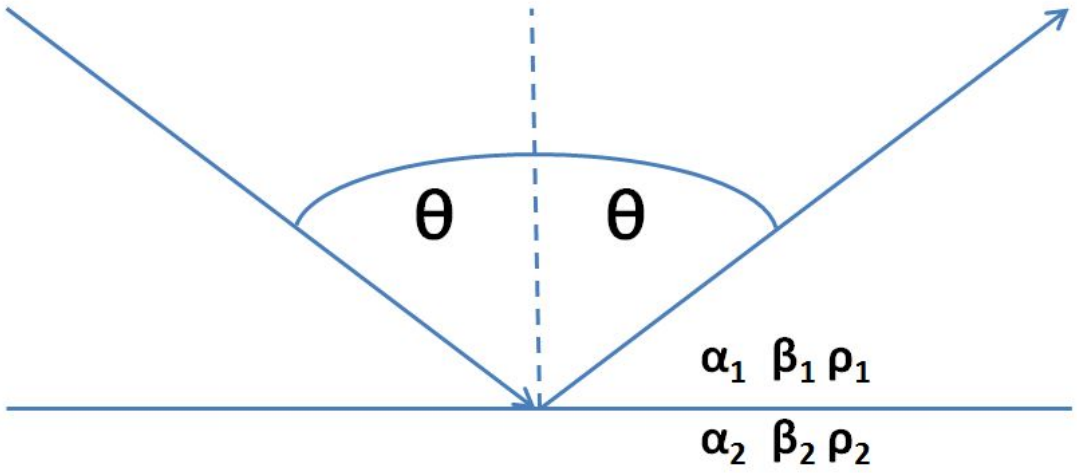

Figure 15: Schematic drawing of a seismic P-wave hitting an interface between with incidence angle θ

$R(0)$ is the reflection coefficient at normal incidence and is often referred to as the intercept, G is called the gradient and controls the variation in reflection amplitude at mid-offset, while F describes the variation in reflectivity at far offset, angles close to the critical angle. Normally when doing amplitude versus offset (AVO) analysis on datasets with incidence angles not exceeding 30-40° the third term, F, is often ignored and the two term Aki-Richards, is rather used:

$$R(\theta) = R(0) + Gsin^2\theta \tag{15}$$

The intercept, R(0), is only dependent on the contrast in acoustic impedance across an interface. The gradient, G, on the other hand is more complex. In addition to be dependent of P-wave velocity and density, also the S-waves contributes to the P-wave reflection coefficient. We can see from Equation 14 that the $\frac{V_p}{V_s}$ ratio plays an important role in determining the value of the gradient. This is essential for the usage of AVO. Gas filled sandstones capped by shale has an very low $\frac{V_p}{V_s}$ ratio compared to nongaseous surrounding formations. This will cause a significantly more negative gradient for reflections on top of a gas filled sandstone compared to a water filled one. A much used technique in interpretations of AVO-responses is plotting the intercept versus gradient in a cross plot. It turns out that one can use this tool to better distinguish between different lithologies and fluid saturations.

As for every other tool used for 4D monitoring of a producing hydrocarbon reservoir it is essential to understand what kind of response various production changes will cause on the AVO signature. Landrø published a paper in 2001 where he derived explicit expressions for computing saturation- and pressure-related changes from time lapse data with near- and far-offset stacks as input (Landrø, 2001). The idea in Landrøs paper was to separate the effect of pore pressure related changes and the effect of saturation related changes in different attribute maps. This can be of advantage when both effects are influencing the seismic difference data at the same time. Landrø addressed the relative variations of seismic parameters to the changes in pressure- and saturation-changes by use of this approximations:

$$\frac{\Delta V_p}{V_p} \approx k_\alpha \Delta S + l_\alpha \Delta P + m_\alpha \Delta P^2 \tag{16}$$

$$\frac{\Delta V_s}{V_s} \approx k_\beta \Delta S + l_\beta \Delta P + m_\beta \Delta P^2 \tag{17}$$

$$\frac{\Delta \rho}{\rho} \approx k_\rho \Delta S \tag{18}$$

where ΔS and ΔP are the changes in oil saturation and net pressure, respectively, and $k_\alpha, k_\beta, k_\rho, l_\alpha, l_\beta, m_\alpha$ and m_β are empirical parameters estimated from for example lab measurement or theoretical models. Here a linear relationship for saturation changes and a quadratic relationship for pressure changes are used. By combining the fluid- and saturation-changes the total change in reflectivity between two seismic

surveys can be written as:

$$\begin{aligned}\Delta R \approx & \frac{1}{2}(k_\rho \Delta S + k_\alpha \Delta S + l_\alpha \Delta P + m_\alpha \Delta P^2) \\ & + \frac{1}{2}(k_\alpha \Delta S + l_\alpha \Delta P + m_\alpha \Delta P^2)\tan^2\theta \\ & - \frac{4{V_s}^2}{{V_p}^2}(l_\beta \Delta P + m_\beta \Delta P^2)\sin^2\theta \end{aligned} \tag{19}$$

By use of the two term Aki-Richards, Equation 15, and assuming relatively small angles so that $\tan\theta \approx \sin\theta$, Equation 19 can be split into an intercept and a gradient part:

$$\Delta R_0 \approx \frac{1}{2}(k_\rho \Delta S + k_\alpha \Delta S + l_\alpha \Delta P + m_\alpha \Delta P^2) \tag{20}$$

$$\begin{aligned}\Delta G \approx & \frac{1}{2}(k_\alpha \Delta S + l_\alpha \Delta P + m_\alpha \Delta P^2) \\ & - \frac{4{V_s}^2}{{V_p}^2}(l_\beta \Delta P + m_\beta \Delta P^2) \end{aligned} \tag{21}$$

By solving this two equations explicit expressions for saturation- and pressure-changes can be derived. The expression for the pressure variation can be written as:

$$\Delta P \approx \frac{-b \pm \sqrt{b^2 - 4ac}}{2a} \tag{22}$$

where

$$a = m_\alpha - \frac{8{V_s}^2}{{V_p}^2}m_\beta - \frac{m_\alpha k_\alpha}{k_\alpha + k_\rho} \tag{23}$$

$$b = l_\alpha - \frac{8{V_s}^2}{{V_p}^2}l_\beta - \frac{k_\alpha l_\alpha}{k_\alpha + k_\rho} \tag{24}$$

$$c = \frac{2k_\alpha \Delta R_0}{k_\alpha + k_\rho} - 2\Delta G \tag{25}$$

In normal situations b in Equation 24 is negative. Since zero values for changes in intercept and gradient should give zero changes in pressure and saturation, the negative root is excluded. In special situations where b is positive, the positive root should be excluded. The corresponding expression for saturation-changes can be written:

$$\Delta S \approx \frac{1}{k_\alpha + k_\rho}(2\Delta R_0 - l_\alpha \Delta P - m_\alpha \Delta P^2) \tag{26}$$

By use of empirical parameters the two different effect has been separated into two different vectors in the R(0)-G cross-plot. This makes it possible to express the two

different effects in a direct way. One should be aware that several assumptions are made to create this attributes. In addition to numerical approximations, assumptions are made that all the changes in pressure and saturation are taking place in the reservoir segment, no changes occur in the cap rock. The variations in seismic parameters are assumed to follow the relations given in Equation 16 to Equation 18. These parameters are generally varying with spatial location and assumptions need to be made that the derived relations are valid for a given area around the location used for calibrating the model.

Figure 16 shows an intercept-gradient cross-plot with different trend lines for fluid, pressure, noise and lithology response.

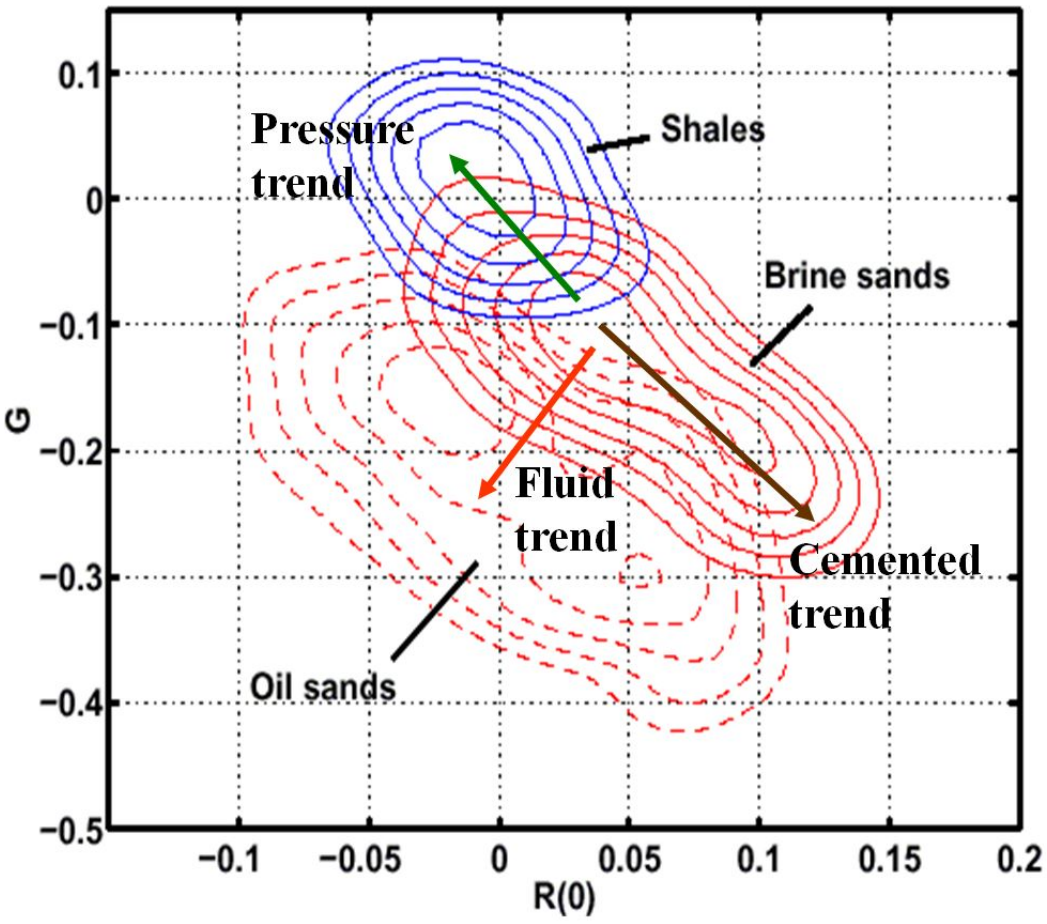

Figure 16: Different AVO trends occurring in an intercept-gradient cross-plot. Modified version of Avseth (2011)

4.1.3 Repeatability and noise

One of the major challenges regarding 4D seismic is to repeat the seismic monitoring surveys as equal to the base survey as possible. How much effort one should put into the acquisition is a question of how sensitive the time-lapse survey needs to be and how complex the geology in the field and the overburden is. Noise, or nonrepeatability, in 4D seismic is normally measured in normalized root-min-square difference (NRMS):

$$NRMS = \frac{2 * rms(T1_t - T2t)}{rms(T1_t) + rms(T2_t)} \tag{27}$$

where $T1$ and $T2$ are the two compared traces and t the time gate the NRMS is measured over (normally a time interval where no production changes are predicted). Various factors have influence on the repeatability (Landrø, 2011):

- Varying source and receiver position
- Change in weather conditions during acquisition
- Varying sea water temperature
- Tidal effects
- Noise from other vessels or other activities in the area (rig noise)
- Varying source signal
- Change in acquisition system (new vessel, other cables, sources, etc.)
- Variation in shot generated noise (from previous shot)

Except the weather and sea water temperature conditions, the key to do a good repeated survey is good planing and accurate operation.

One of the most crucial part regarding repeatability is to repeat the source and receiver position as good as possible, specially in places with complex geology. For a given reflection point only a small variation in source and/or receiver position from one vintage to another can lead to big seismic differences even at places where nothing has changed. A powerful way to illustrate this is the use of variograms where the trace nonrepeatability is plotted as a function of geometric difference. Figure 17 shows a variogram from a VSP experiment Norsk Hydro did over the Oseberg Field, North Sea. 10000 shots were acquired in a circular shooting pattern and recorded by fixed receivers in the well. The variogram shows 70000 shot pairs and one can clearly see that the trace nonrepeatability is increasing as the geometric

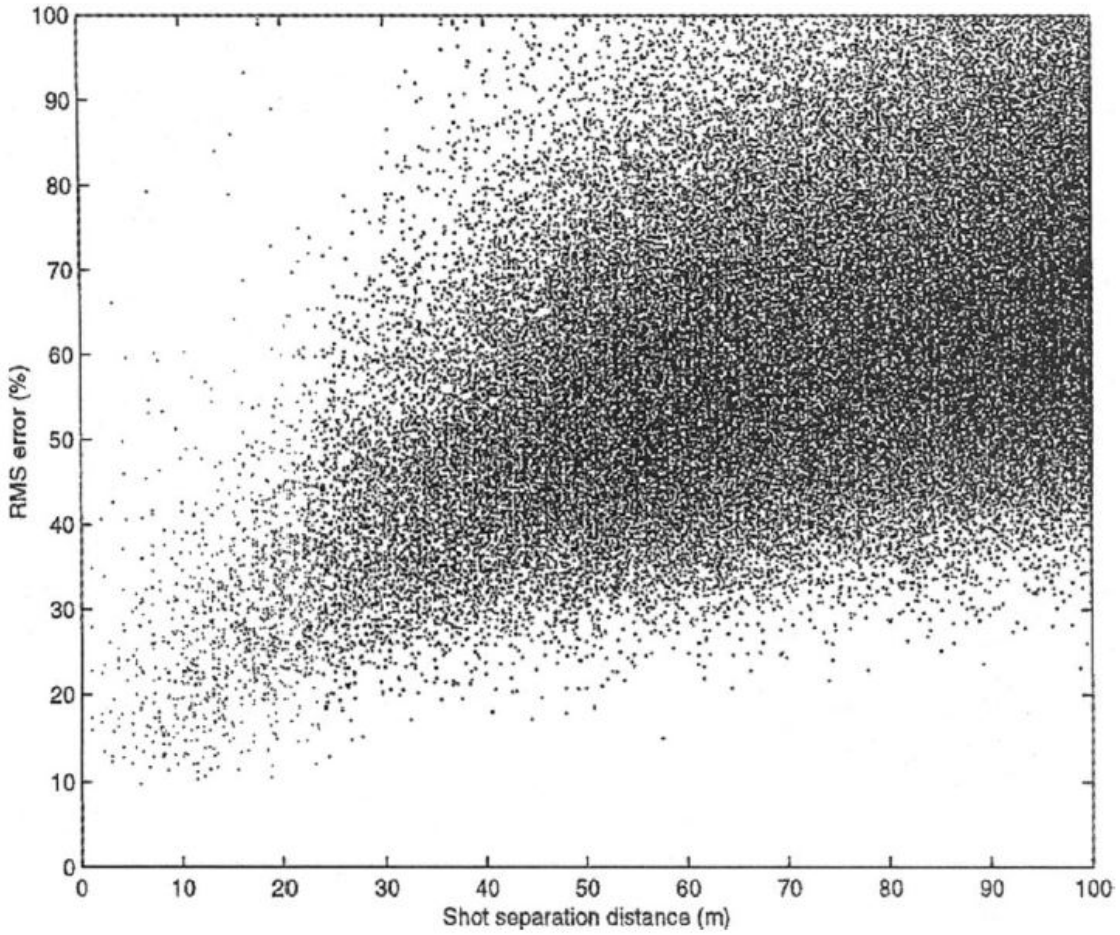

Figure 17: The trace nonrepeatability, measured in NRMS, plotted as a function of geometry difference in a variogram. Each point corresponds to one pair of shots. The overall trend of increased error with increased separation distance is clear. From Landrø (1999)

difference is increasing. If we look at a given geometric difference the NRMS value spans over a wide range. For example on a geometric difference of 30 meters, the NRMS values spans form 20 % and all the way up to around 80 %. A large portion of this variations can be addressed to the difference in geology from one shot pair to another (Landrø, 1999).

5 Methods

The seismic interpretation software Petrel 2012.3 (64-bit) developed by Schlumberger was used for the interpretation of most of the seismic data. Only the work done regarding amplitude versus offset was done using the Hampson-Russell Suite Version 9 (HRS-9/R-1.4.1) software developed by CGG. Matlab R2013a were used to create plots in the theory part.

5.1 Seismic horizons

Top Springar Formation The top Springar Formation was interpreted using *2D autotrack* and *3D autotrack* in Petrel. The horizon was mainly interpreted to control for static time shifts in the overburden.

Top Garn Formation The top Garn Formation defines the top of the Norne reservoir. The basis for the horizon was imported from the *Norne Full Field Database* coordinated by the Center for Integrated Operations at NTNU. Petrel *2D autotrack* and *3D autotrack* with the imported horizon as constrain was used to map the horizon in all the different vintages. The *Surface* process in Petrel was used to make surfaces of the mapped horizons.

Top Åre Formation The top Åre Formation defines the base of the main reservoir at Norne. The basis for the horizon was imported from the *Norne Full Field Database*. The horizon was mapped and converted to surfaces in the same way as the top Garn Formation.

Below reservoir A horizon below the reservoir was interpreted using *2D guided autotrack* in Petrel. A dense net of interpreted in-lines and cross-lines was interpreted and converted to surfaces by use of the *Surface* process in Petrel. The horizon was interpreted in all the different seismic vintages and made a basis for the time shift analysis.

5.2 Amplitude and amplitude difference maps

The amplitude maps and the amplitude difference maps in this thesis was made using the *Surface attribute* process and the *Calculator* in Petrel. The *mean amplitude*

attribute was used to create amplitude maps on surfaces in different vintages. The *Calculator* was used to subtract one amplitude map in one vintage from another amplitude map in another vintage to create amplitude difference maps between the two vintages.

5.3 Time shift maps

Time shift maps for top Springar Formation, top Garn Formation and for a seismic reflector below the reservoir was made using the *Surface attribute* process in Petrel. The *Isochron thickness* attribute was used to measure a surface's shift in time between different seismic vintages. The time shift maps for the top Springar Formation and the top Garn Formation was created to control for static time shifts in the overburden. Due to very low values of static time shifts in the overburden no corrections were performed to compensate for these shifts.

5.4 AVO analysis

5.4.1 Using near-, mid- and far-stack seismic data as pre stack data

For the amplitude versus offset analysis part in this thesis a merged seismic cubes were created by merging the near-, mid- and far-stack data into angle gather volumes. The merged volumes were later treated as a pre-stack datasets in the AVO analysis workflow in the Hampson-Russell software. Due to lack of offset data for each trace in the different angle stacks a mean angle was set in the header for all the traces in the stacks. All the traces in the near-stacks were set to have an incidence angle of 10°, which is the mean of the highest and lowest angles in the near-stacks, all mid-stack traces were set to have an incidence angle of 22.5° while all far-stack traces were set to have an incidence angle of 35°.

Regression to best fit the near-, mid-, and far-stack data to the two term Aki-Richards equation, Equation 15, was used to create intercept- and gradient-cubes for all the four merged volumes, Figure 18.

5.4.2 Saturation- and pore pressure-change attribute maps

Landrø's method for discriminating pressure-related changes from saturation-related changes in seismic data (Landrø, 2001) was used to create attribute maps for saturation-

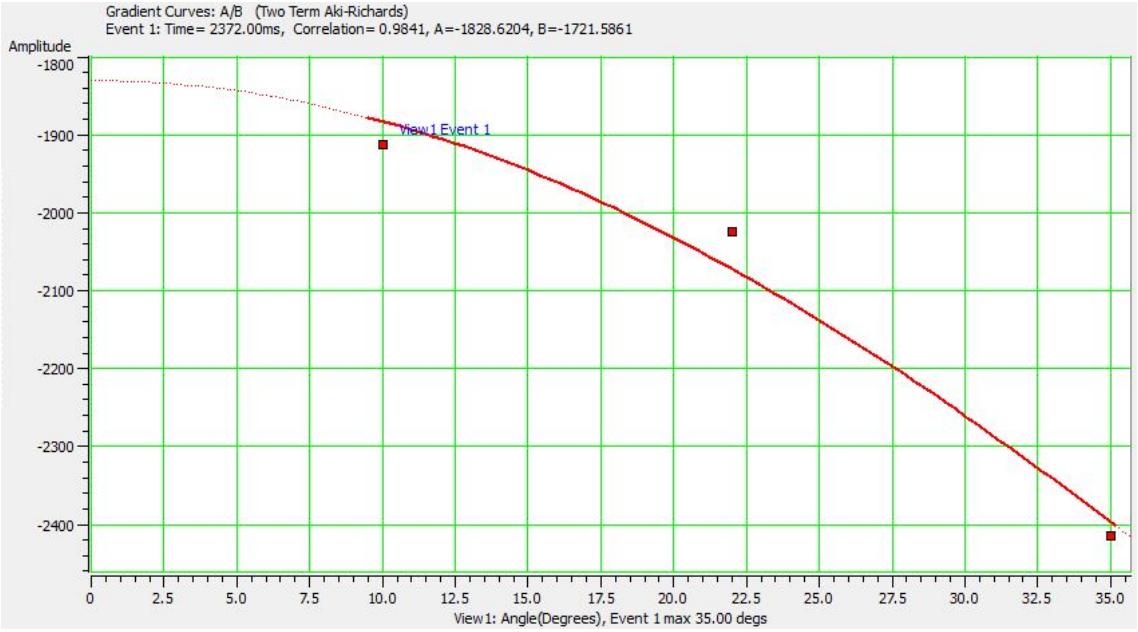

Figure 18: Creation of reflection curve by use of regression to best fit the near-, mid-, and far-stack data to the two term Aki-Richards equation

and pore pressure-changes. The rock physics analysis published by Osdal et al. (2006), Figure 32, has been used as a base when deriving the relations between changes in seismic velocities and the changes in pressure and saturation. The following relations were extracted from the P-wave velocity versus saturation plot, Figure 32(b):

$$\begin{aligned} \frac{\Delta V_p}{V_p} &\approx k_\alpha \Delta S \\ \frac{\Delta 70}{2910} &\approx 0.175 k_\alpha \\ \Rightarrow k_\alpha &= 0.1375 \end{aligned} \tag{28}$$

From the P-wave velocity versus pressure plot, Figure 32(a), the following relations were derived:

$$\begin{aligned} \frac{\Delta V_p}{V_p} &\approx k_\alpha \Delta S + l_\alpha \Delta P + m_\alpha \Delta P^2 \\ -\frac{40}{2940} &\approx 10 l_\alpha + 10^2 m_\alpha \\ -\frac{340}{2940} &\approx 20 l_\alpha + 20^2 m_\alpha \\ \Rightarrow l_\alpha &= 0.0224 \qquad m_\alpha = -0.0011 \end{aligned} \tag{29}$$

By assuming the $\frac{V_p}{V_s}$ to be constant and unaffected by the changes in pore pressure:

$$l_\beta = l_\alpha \qquad m_\beta = m_\alpha \tag{30}$$

The empirical constant for the relation between saturation- and density changes were calculated using assumed densities for gas, $\rho_g = 200kg/m^3$, and matrix, $\rho_m = 2.65$, and a porosity of 30%, $\phi = 0.3$:

$$\begin{aligned} \frac{\Delta\rho}{\rho} &\approx k_\rho \Delta S \\ \frac{42}{2155} &\approx 0.175 k_\rho \\ \Rightarrow k_\rho &= 0.1114 \end{aligned} \tag{31}$$

The last constant k_β was assumed to be equal to -0.03.

By inserting this to Equation 22 and Equation 26 the following expressions for pressure and saturation changes were derived:

$$\Delta P \approx 32\Delta R_0 - 57\Delta G \tag{32}$$

$$\Delta S \approx 5(\Delta R_0 + \Delta G) \tag{33}$$

Pore pressure-change attribute maps and saturation-change attribute maps were created using the *Create AVO Attribute Data Slice* and the *Combine two data slices* processes in the Hampson-Russell software.

6 Results

6.1 2001

Figure 19 shows a seismic section of a random line going through the C- and G-segment of the Norne Field. The line is crossing exploration well 6608/10-2 and 6608/10-4, injection well 6608/10-F-4 and is going along production well 6608/10-E-4, the line is marked yellow in Figure 20. Interpretations of Top Springar Formation, Top Garn Formation and Top Åre Formation are included in the seismic section. We can see that the top reservoir, the Top Garn Formation, is represented by a clearly defined soft event in the seismic section as a result of transition from tight Upper Jurassic carbonaceous claystones of the Melke Formation to the hydrocarbon bearing middle Jurassic sandstones of the Garn Formation. Also the base reservoir boundary for the main field, the Top Åre Formation, is represented by a soft seismic event as it lies at the boundary between the good quality reservoir sandstones of the Tilje Formation and the carbonaceous and calcareous sandstones of the Åre Formation. The white interpreted line right below the Top Garn Formation is an approximate position of the Not Formation which defines the base of reservoir interval in the G-segment.

As a side note, a quick examination of the seismic section we can clearly see the thinning of the reservoir interval between Top Åre Formation and Top Garn formation to the north which suport the theory of episodic uplift and increased erosion to the north during Lower to Middle Jurassic time as described in subsection 2.1. This is out of scope for this thesis and will not be further discussed here.

Figure 20 shows mean amplitude map of Top Garn Formation in 2001. In the reservoir segments the horizon is a clear, high amplitude negative seismic event indicating a distinct drop in acoustic impedance on Top Garn Formation. The highest amplitudes are observed in the highest elevated sections of the main field and in the G-segment. The area between the C- and G-segment, reffered to as the saddle area, and the areas outside the main horst block shows lower amplitudes, allmost zero to positive. The transition from high negative amplitudes to the lower amplitudes seems to line up good with the time-contours of the Top Garn Formation.

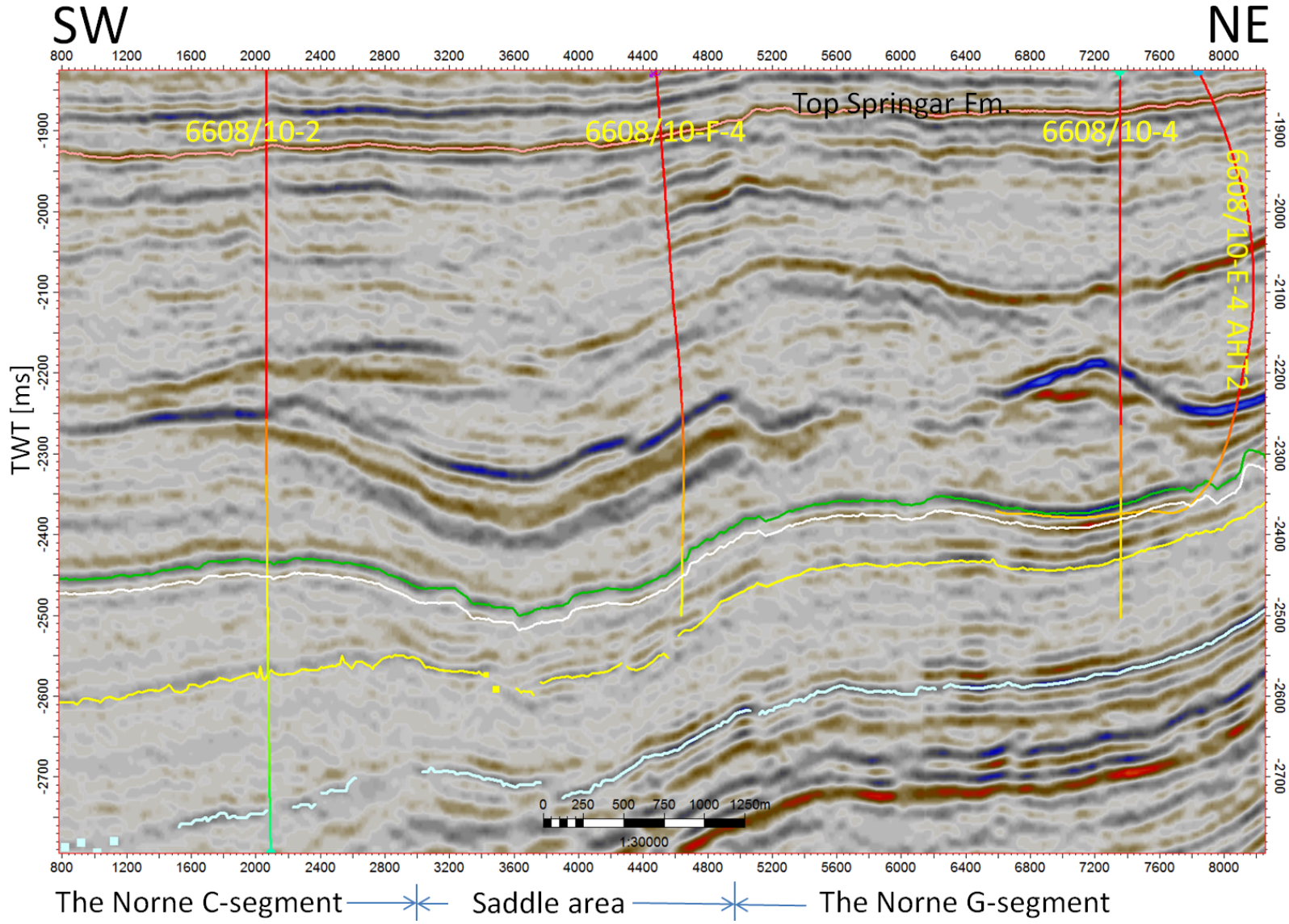

Figure 19: Seismic section going through the C- and G-segment in the Norne Field. Exploration wells 6608/10-2, 6608/10-4, production well 6608/10-E-4 and injection well 6608/10-F-4 are included. Pink interpreted horizon is Top Springar Formation, green interpreted horizon is Top Garn Formation, white interpreted line gives the approximate position of the Top Not Formation, yelow interpreted horizon is Top Åre Formation. The strong negative reflector below the reservoir is used for time shift calculations, light blue interpreted line

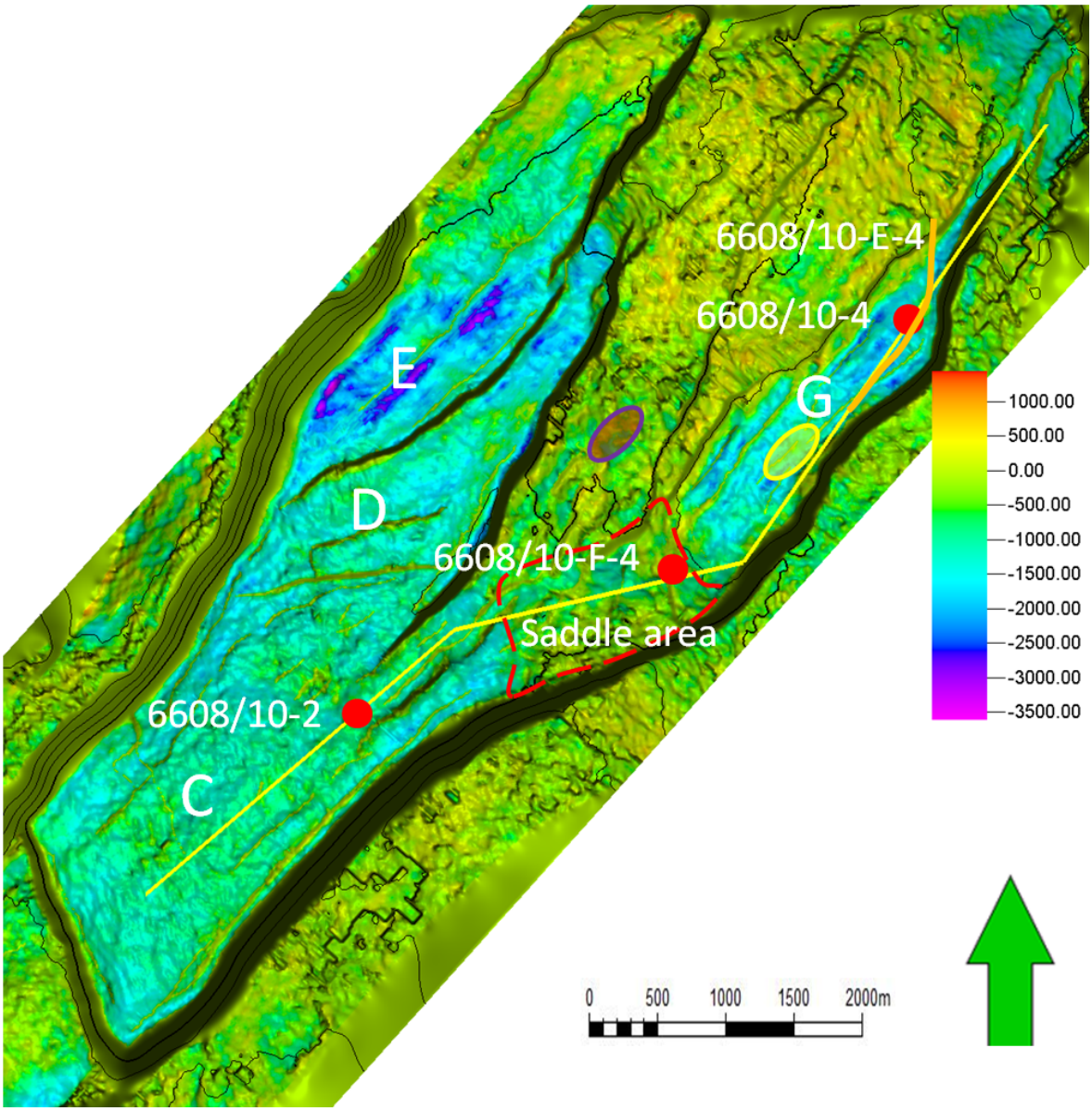

Figure 20: Map showing mean amplitude on Top Garn Formation in 2001. In the reservoir segments, C, D, E and G, the horizon is a clear, high amplitude negative seismic event while in the saddle area between the D- and G-segment and and outside the main horst block the amplitude and smoothness of the horizon is weaker. Yellow and purple circles marks the position of zones where data are collected for cross-plotting in the discussion section, red dots marks well positions

6.2 2003

Figure 21(a) shows change in amplitude on Top Garn Formation between the 2001 and 2003 surveys. Blue is related to a more negative amplitude and red is a more positive amplitude in 2003 compared to 2001. The figure clearly shows a zone with negative amplitude difference around injector 6608/10-F-4 and up along the western main fault. In the north-eastern part of the segment, around producer 6608/10-E-4 and along the eastern main fault, the amplitude response is the opposite as around the injector.

Figure 21(b) shows the pore pressure-change attribute map for Top Garn Formation between 2001 and 2003. Blue is related to a increase in the pore pressure attribute while red is decreased pore pressure attribute in 2003 compared to 2001. The attribute map contains noise so a clear anomaly is hard to locate, but we can see a trend of increased values for the pore pressure attribute around the injector, up along the western main fault and into the north-eastern part of the G-segment, around the location of the heal of producer 6608/10-E-4.

Figure 22(a) shows the saturation-change attribute map for Top Garn Formation between 2001 and 2003. Blue is increase in saturation-change attribute which is related to a change in saturation from an incompressible fluid mixture to a more easily compressible fluid mixture, i.e. increased gas saturation in a mix of gas and water, while red is related to a change in the opposite direction. An anomaly of decreased saturation attribute can be seen in the main part of the G-segment, around the producer 6608/10-E-4 and following the eastern main fault. The anomaly is covering approximately the same area that the increased amplitude anomaly is covering.

Figure 22(b) shows time shifts from the 2001 to the 2003 surveys for a horizon below the reservoir. Red is positive time shifts, meaning that the reflector is shifted to a later time, blue is negative shifts. The figure shows a small anomaly of positive time shifts, up to 2 ms, around injector 6608/10-F-4 and in the direction of the western main fault. The rest of the segment shows no measurable time shifts.

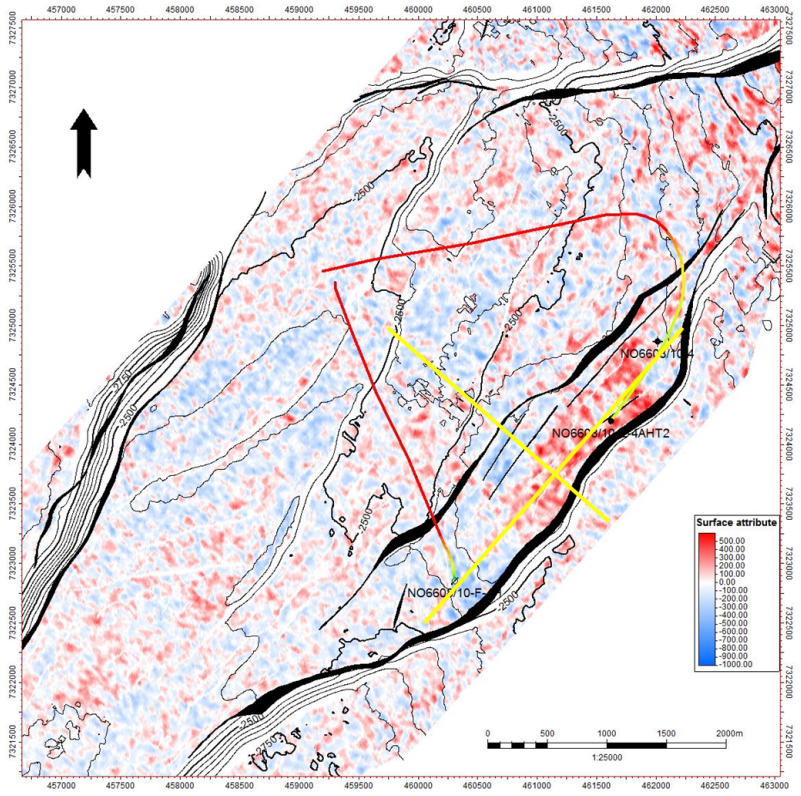

(a) 4D amplitude difference map, 2001 to 2003

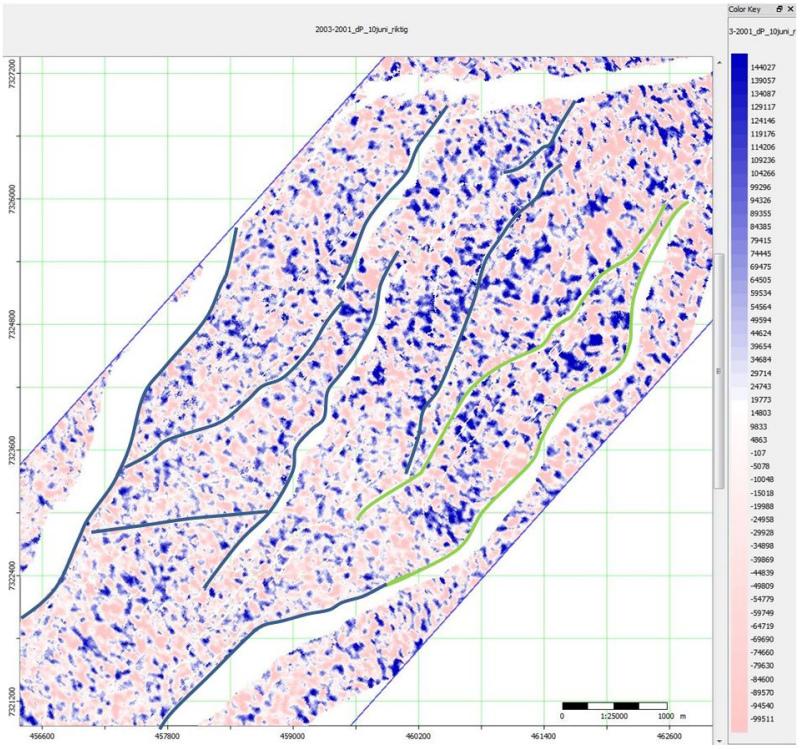

(b) Pore pressure-change attribute map, 2001 to 2003

Figure 21: a): 4D amplitude difference map showing the change in amplitude on Top Garn Formation between the 2001 and 2003 surveys. Blue is related to amplitude decrease and red to an increase in amplitude. Position of well 6608/10-4, injector 6608/10-F-4 and producer 6608/10-E-4 are included. Yellow lines marks positions of in-line 1237 and cross-line 1940. **b):** Pore pressure-change attribute map showing the change in pore pressure attribute on Top Garn Formation between the 2001 to 2003 surveys. Blue is related to an increase in the pore pressure attribute, red to a decrease

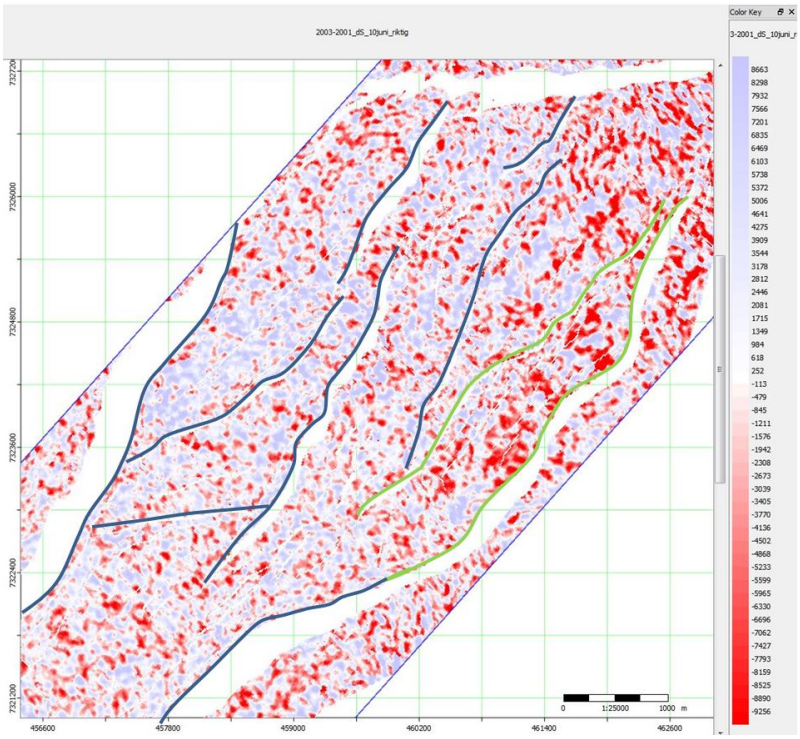

(a) Saturation-change attribute map, 2001 to 2003

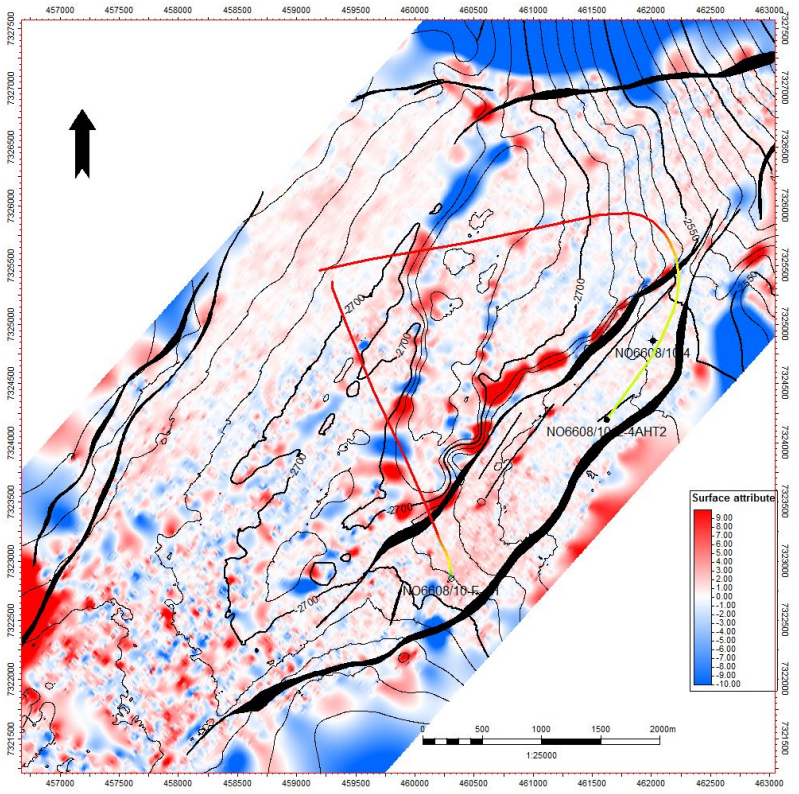

(b) Time shift map, 2001 to 2003

Figure 22: a): Saturation-change attribute map for Top Garn Formation between the 2001 to 2003 surveys. Blue is increase in saturation-change attribute which is related to a change in saturation from an incompressible fluid mixture to a more easily compressible fluid mixture, i.e. increased gas saturation in a mix of gas and water, while red is related to a change in the opposite direction. **b):** Time shift map showing time shifts for a reflector below the reservoir from 2001 to 2003. Red is positive time shift, meaning that the horizon is shifted to a later time, blue is negative time shifts

6.3 2004

Figure 23(a) and Figure 23(b) shows the change in amplitude on Top Garn Formation from 2001 to 2004 and from 2003 to 2004, respectively. We can see from the 2001 to 2004 amplitude difference map that the negative amplitude difference anomaly has propagating further up along the western main fault and that it has been stronger in the area covered by the anomaly on the 2001 to 2003 amplitude difference map. The positive amplitude difference anomaly on the other hand has generally got weaker. On the 2003 to 2004 amplitude difference map a negative amplitude difference in most of the segment is observed except an area around the toe of the producer. This area shows a positive amplitude difference between the 2003 and 2004 surveys, blue circle in Figure 23(b).

Figure 24(a) and Figure 24(b) shows the pore pressure-change attribute map for Top Garn Formation for the 2001 to 2004 and for the 2003 to 2004 surveys, respectively. The 2001 to 2004 attribute maps shows a clear increase in the pore pressure attribute anomaly around the producer and up along the western main fault. The 2003 to 2004 attribute map shows a weak trend of increased amplitude attribute in the same areas as the 2001 to 2004 attribute map, but noise in the attribute map makes it hard to identify the outline of this anomaly.

Figure 25(a) and 25(b) shows the saturation-change attribute map for Top Garn Formation for the 2001 to 2004 and for the 2003 to 2004 surveys, respectively. The negative saturation-change attribute anomaly seen between the 2001 an 2003 surveys is also seen on the 2001 to 2004 attribute map, the 2003 to 2004 attribute map shows no detectable changes.

Figure 26(a) and Figure 26(b) shows the time shifts between the 2001 to 2004 survey and between 2003 to 2004, respectively. From the 2001 to 2004 map we can see that the positive time shift around the the injector and up along the western main fault has been stronger and growth in extent. Time shifts close to the injector are approximately 3 ms. The anomaly is covering an area from down south-west in the saddle area to approximately the toe of producer 6608/10-E-4. The figure also shows a clear positive time shifts around and between the injectors in the E-segment, green circles in Figure 26(a).

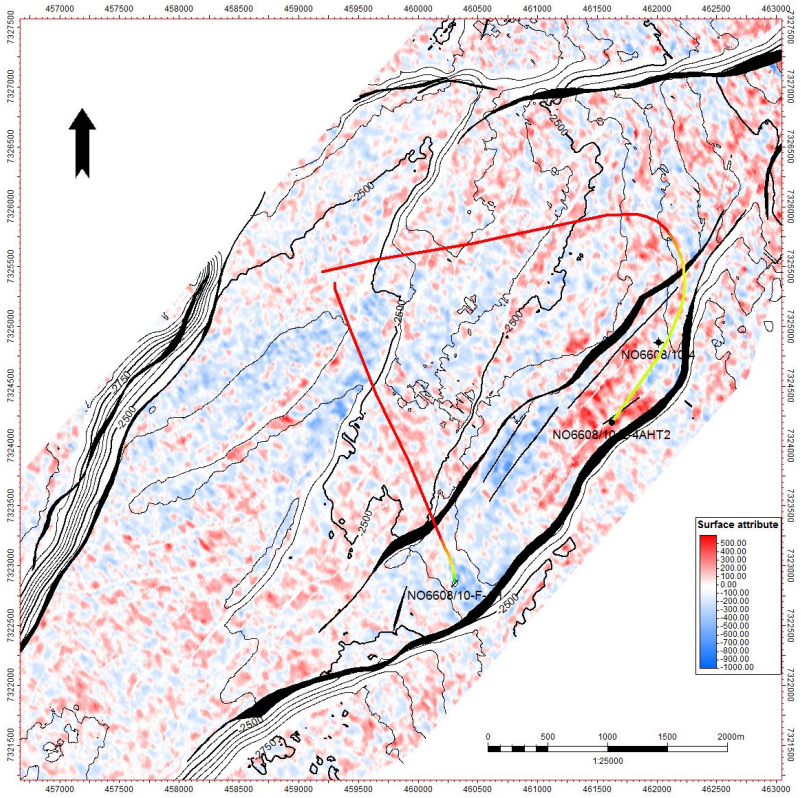

(a) 4D amplitude difference map, 2001 to 2004

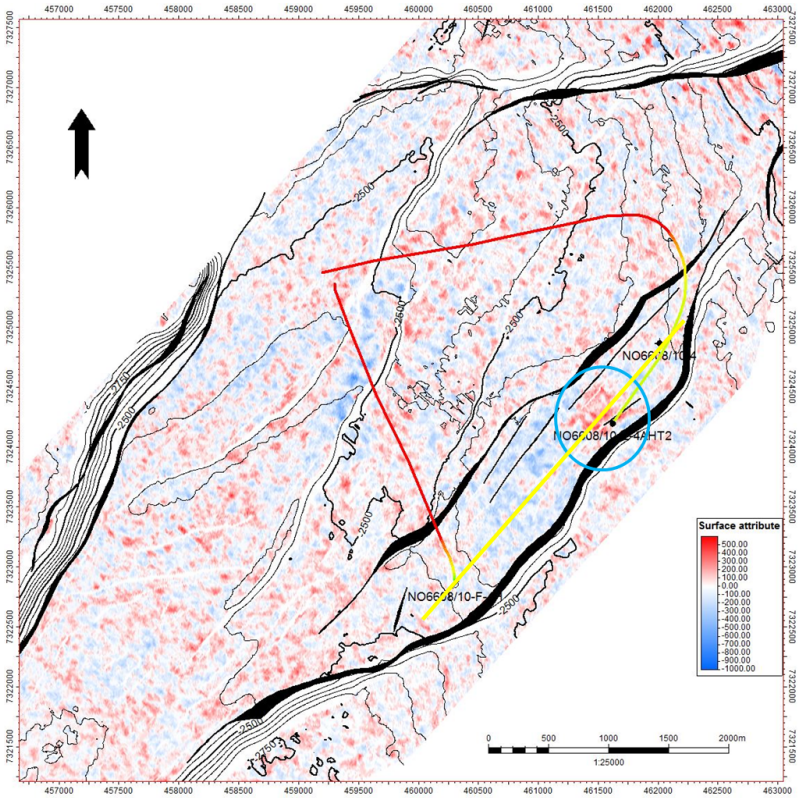

(b) 4D amplitude difference map, 2003 to 2004

Figure 23: 4D amplitude difference maps showing the change in amplitude on Top Garn Formation between the **a)** 2001 and 2004 and **b)** 2003 and 2004 surveys. Blue circle in b) marks an anomaly of positive amplitude difference between the 2003 and 2004 surveys while yellow line marks the position of in-line 1227

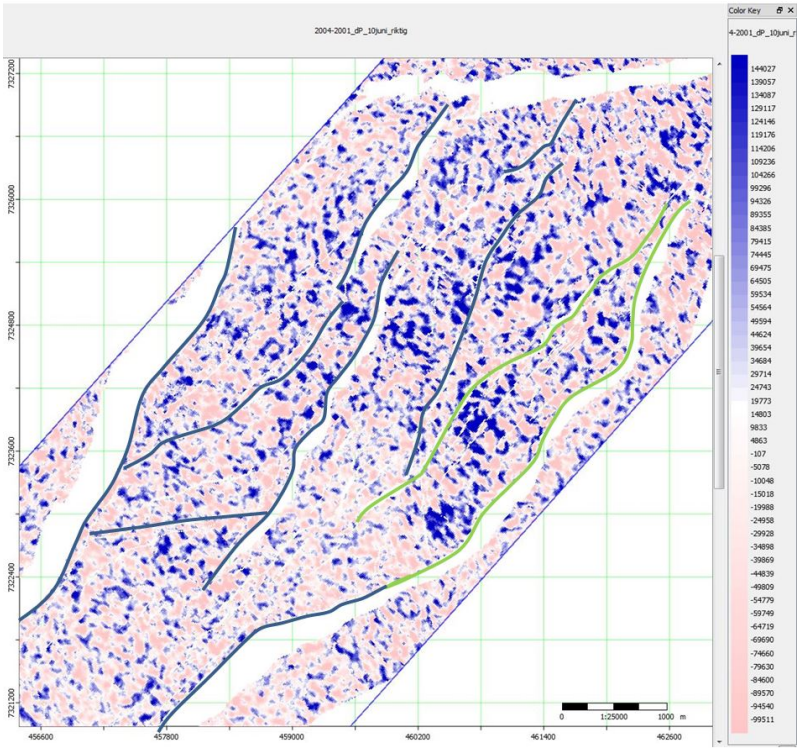

(a) Pore pressure-change attribute map, 2001 to 2004

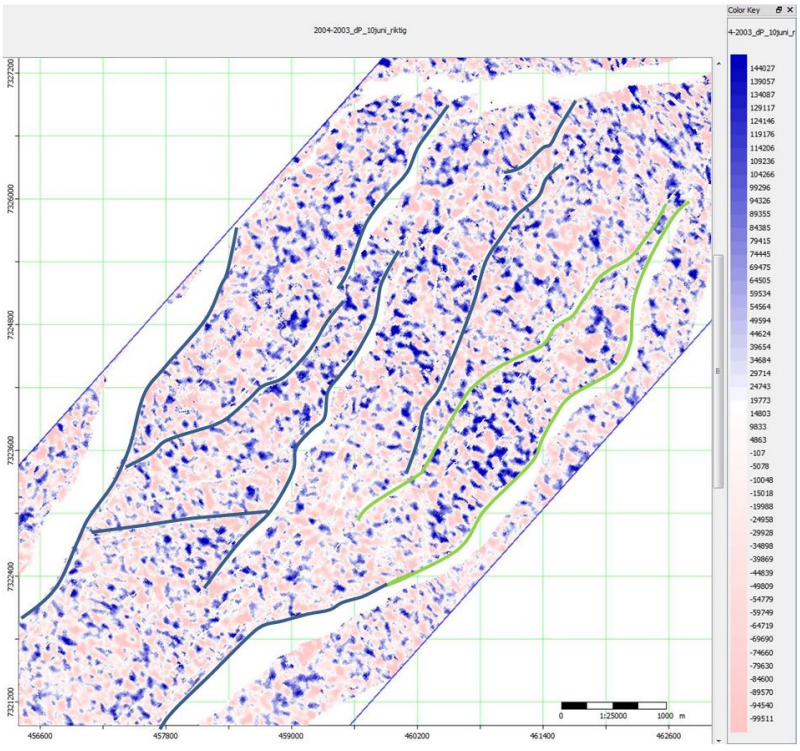

(b) Pore pressure-change attribute map, 2003 to 2004

Figure 24: Pore pressure-change attribute maps showing the change in pore pressure attribute on Top Garn Formation between the **a)** 2001 and 2004 and **b)** 2003 and 2004 surveys

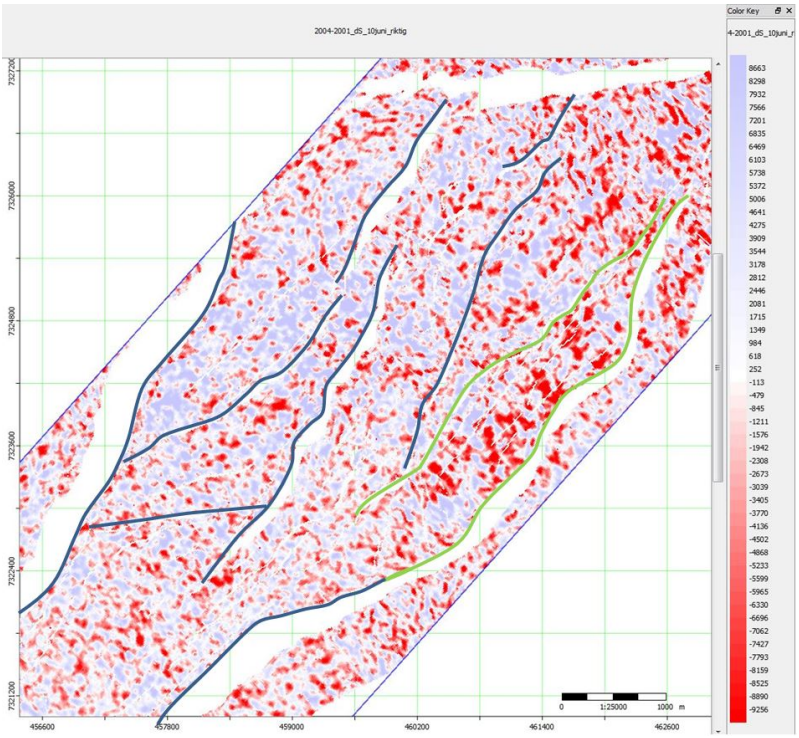

(a) Saturatuin-change attribute map, 2001 to 2004

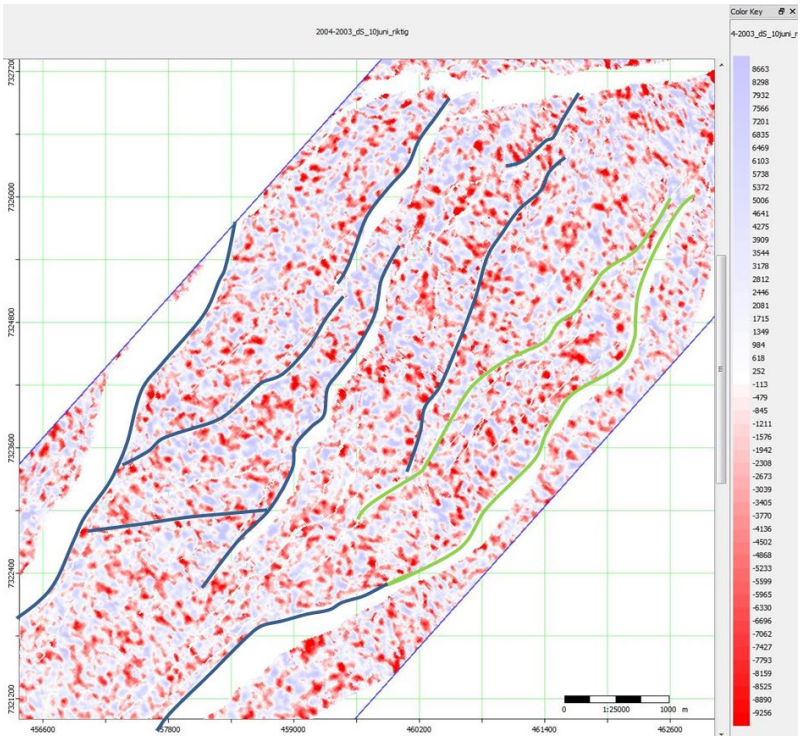

(b) Saturation-change attribute map, 2003 to 2004

Figure 25: Saturation-change attribute maps for Top Garn Formation between the **a)** 2001 and 2004 and **b)** 2003 and 2004 surveys

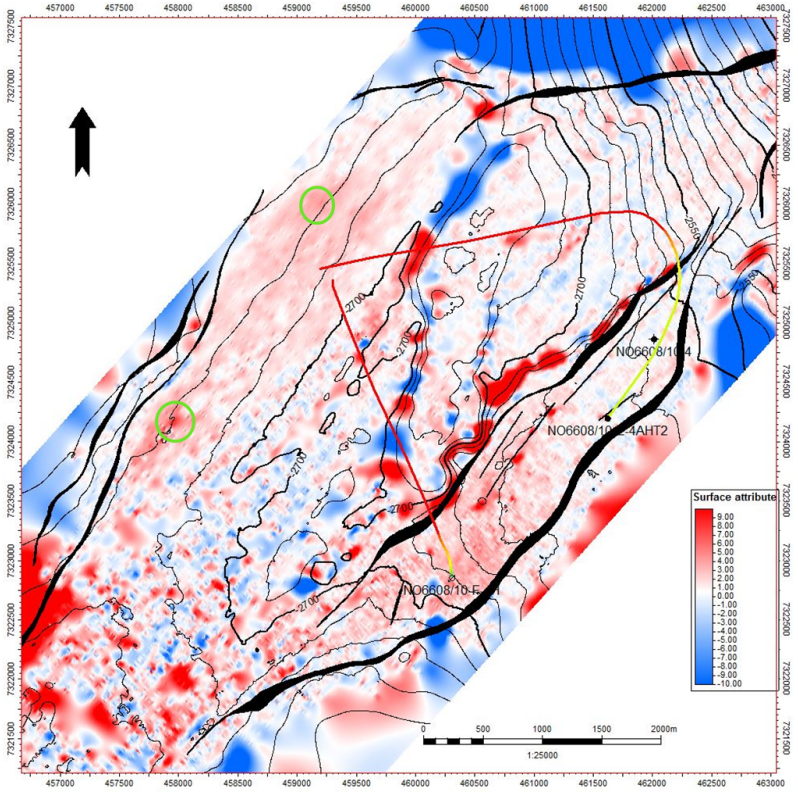

(a) Time shifts from 2001 to 2004

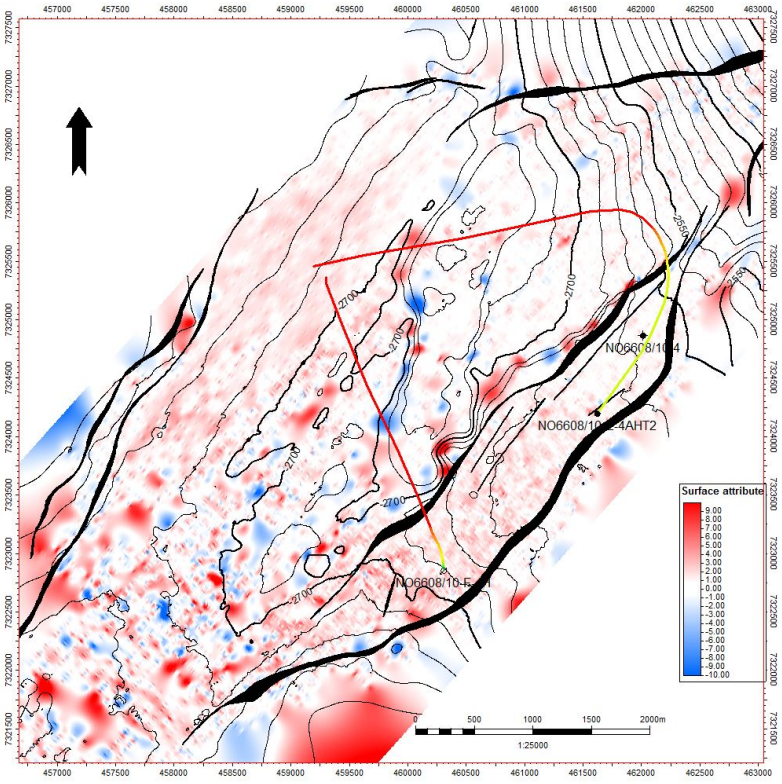

(b) Time shifts from 2003 to 2004

Figure 26: Time shift maps showing time shifts for a reflector below the reservoir from **a)** 2001 to 2004 and **b)** 2003 to 2004. Green circles in a) represents the positions for the water injectors in the E-segment

6.4 2006

Figure 27(a) and Figure 27(b) shows the amplitude change from 2001 to 2006 and 2004 to 2006, respectively. The negative amplitude difference anomaly can be seen all the way from the area around injector 6608/10-F-4, up along the western main fault and, new in 2006, the anomaly is also observed in the north-eastern part of the G-segment, around the heal of producer 6608/10-E-4. The positive amplitude anomaly in the rest of the segment is smaller in extent and less positive compared to the 2001 to 2003 and 2001 to 2004 amplitude difference maps.

Figure 28(a) and Figure 28(b) shows the pore pressure-change attribute map for Top Garn Formation for the 2001 to 2006 and for the 2004 to 2006 surveys, respectively. The 2001 to 2006 attribute maps shows a clear increase in the pore pressure attribute anomaly around the producer and up along the western main fault. The anomaly has growth in extent and is covering also the north-eastern part of the G-segment. Only a small area close to the eastern main fault is showing minor changes in the pore pressure attribute between 2001 and 2006. The 2004 to 2006 pore pressure-change attribute map shows that the increase in the pore pressure attribute mainly occurs in the north-eastern part of the segment.

Figure 25(a) and Figure 25(b) shows the saturation-change attribute for the 2001 to 2006 and 2004 to 2006 surveys. The negative saturation-change anomaly seen on the 2001 to 2003 attribute map is also seen on the 2001 to 2006 saturation-change attribute map, while the 2004 to 2006 map shows no clear anomalies.

Figure 30(a) and Figure 30(b) shows the time shifts from 2001 to 2006 and from 2004 to 2006, respectively. The positive time shift anomaly is covering most of the G-segment. Time shifts around injector 6608/10-F-4 are measured to approximately 3.5 ms. The main change in time shifts from 2004 to 2006 is the negative time shifts in the north-western part of the segment.

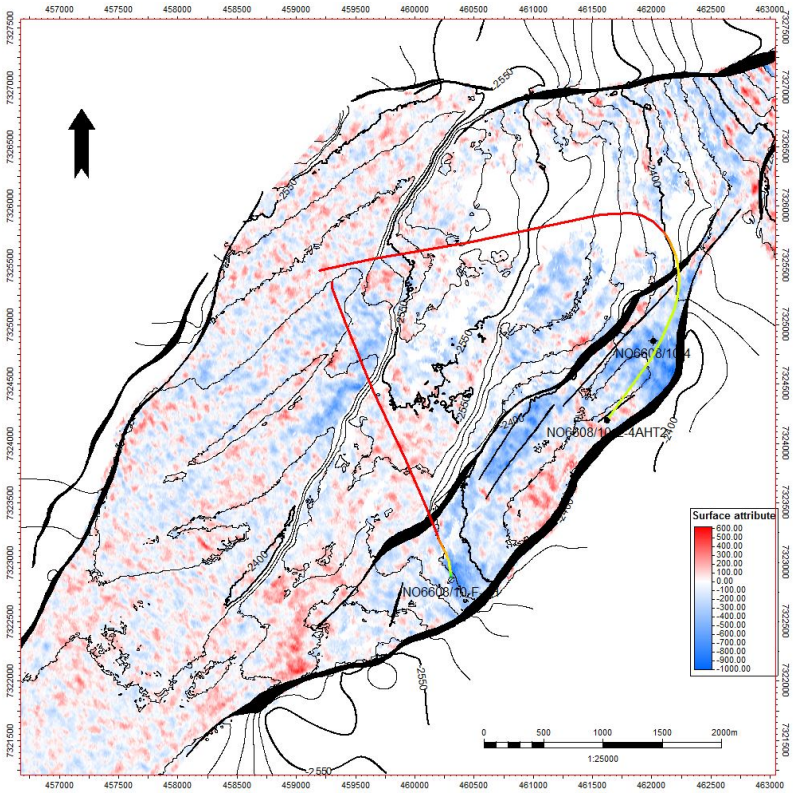

(a) 4D amplitude difference map, 2001 to 2006

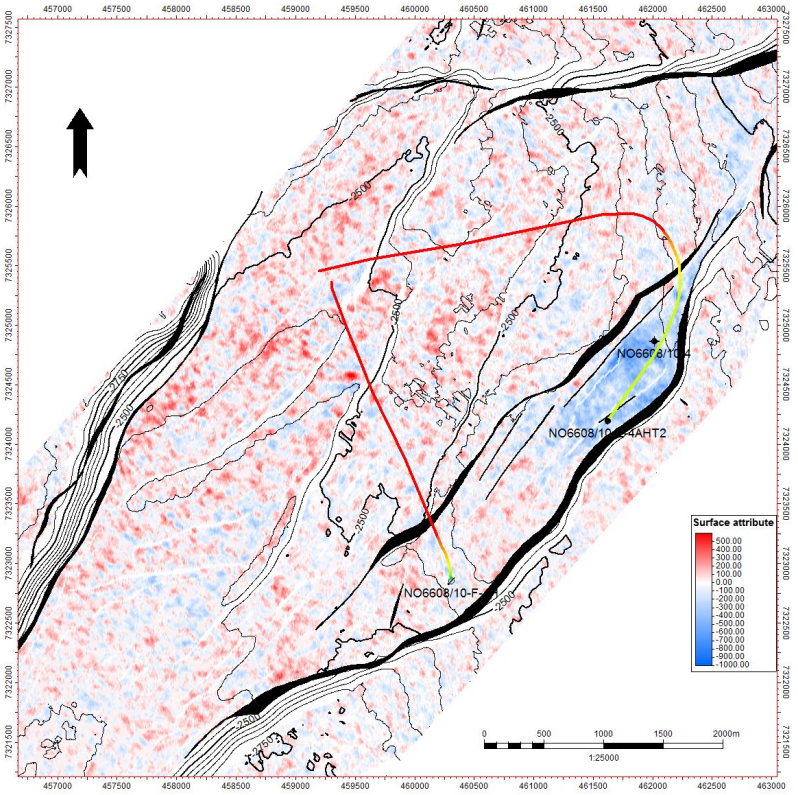

(b) 4D amplitude difference map, 2004 to 2006

Figure 27: 4D amplitude difference maps showing the change in amplitude on Top Garn Formation between the **a)** 2001 and 2006 and **b)** 2004 and 2006 surveys

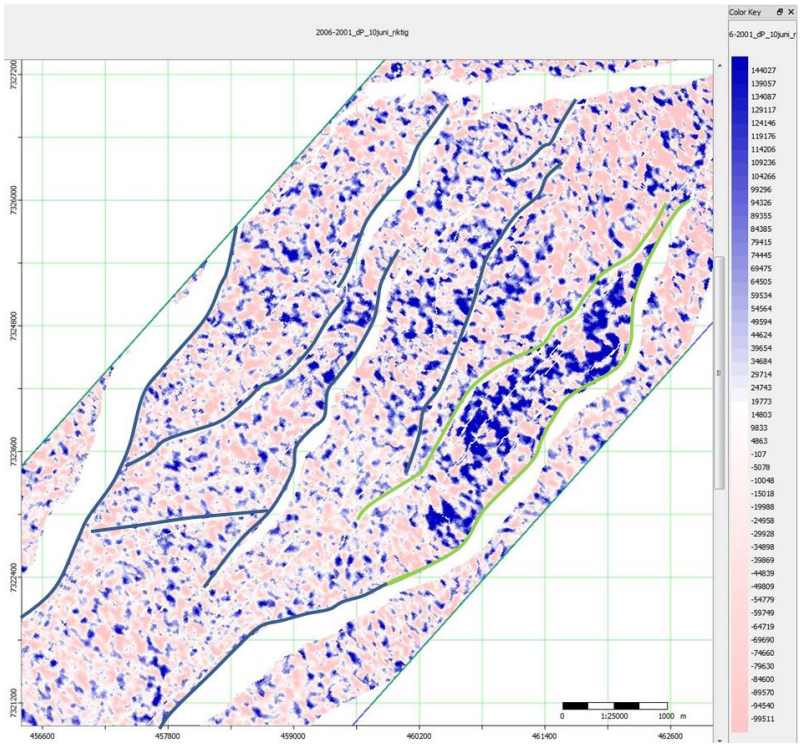

(a) Pore pressure-change attribute map, 2001 to 2006

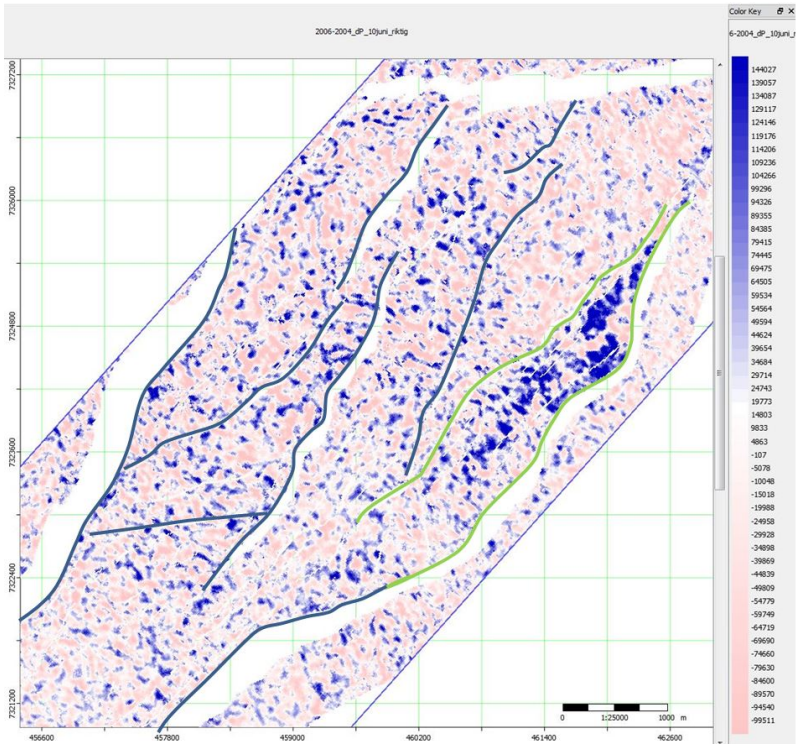

(b) Pore pressure-change attribute map 2004 to 2006

Figure 28: Pore pressure-change attribute maps showing the change in pore pressure attribute on Top Garn Formation between the **a)** 2001 to 2006 and **b)** 2004 to 2006 surveys

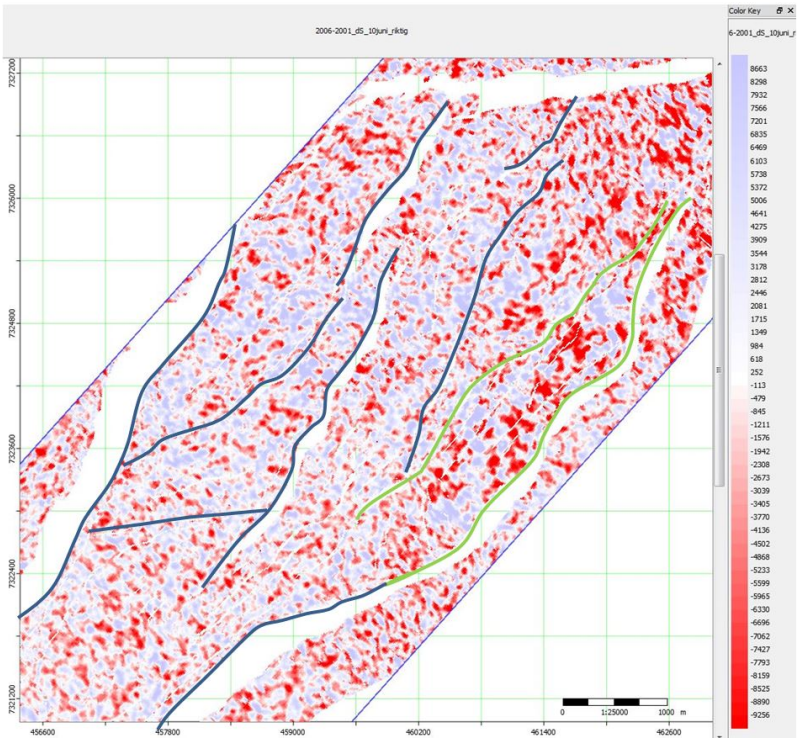

(a) Saturatuin-change attribute map, 2001 to 2006

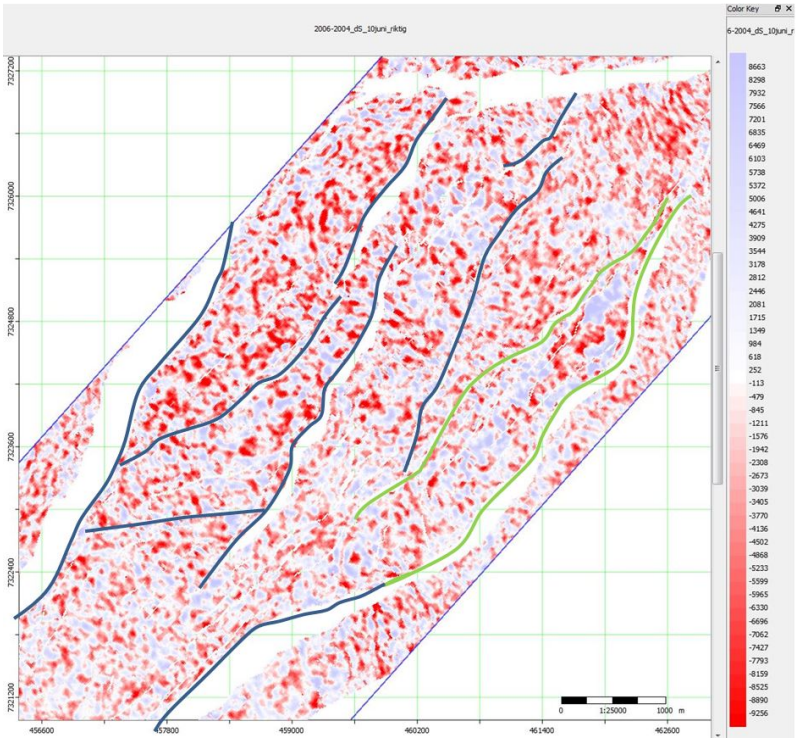

(b) Saturation-change attribute map, 2004 to 2006

Figure 29: Saturation-change attribute maps for Top Garn Formation between the **a)** 2001 to 2006 and **b)** 2004 to 2006 surveys

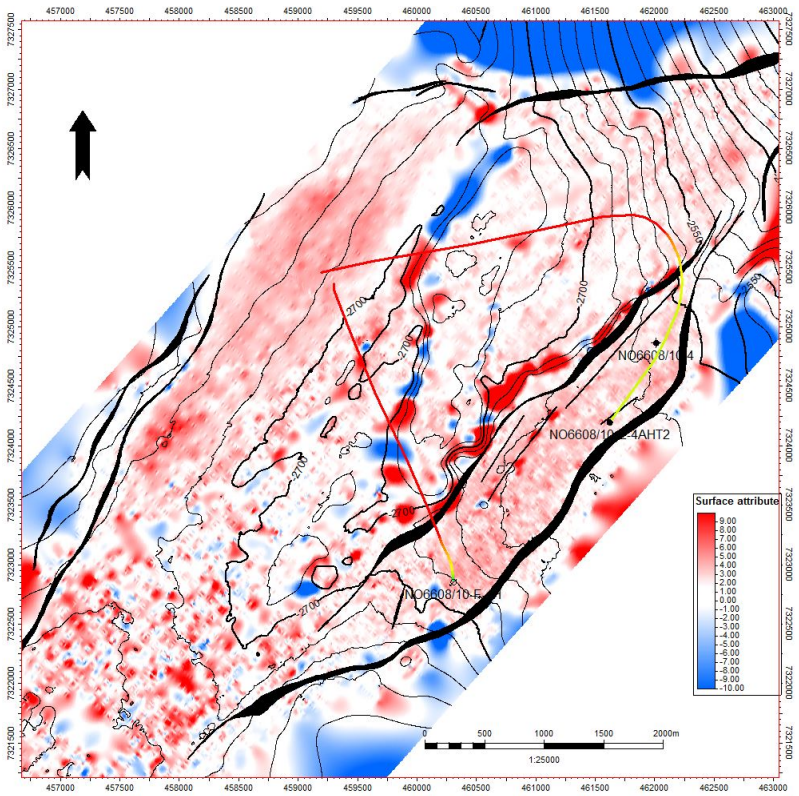

(a) Time shifts between 2001 and 2006

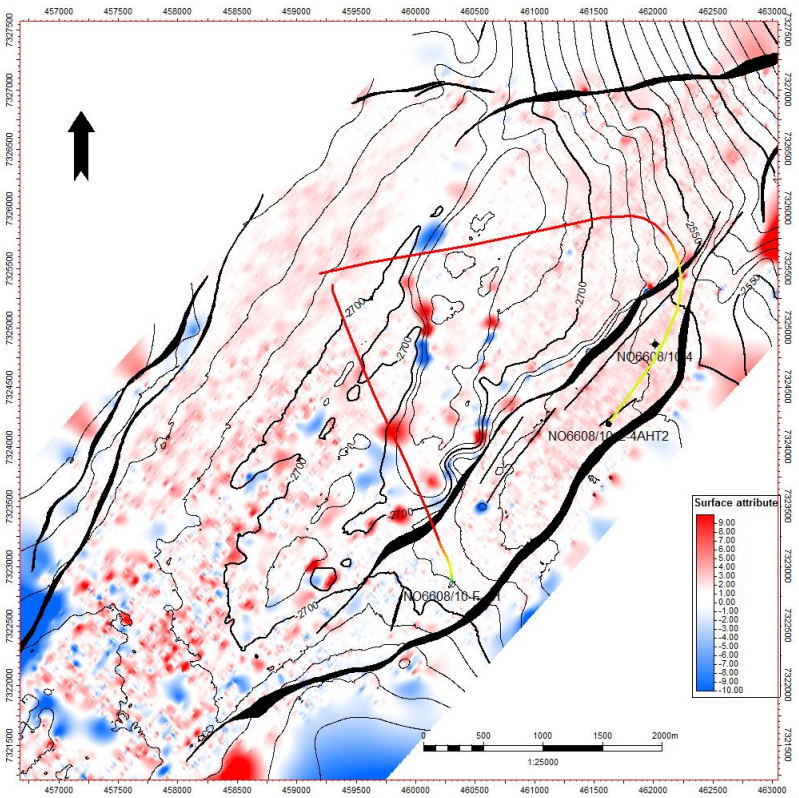

(b) Time shifts between 2004 and 2006

Figure 30: Time shift maps showing time shifts for a reflector below the reservoir from **a)** 2001 to 2006 and **b)** 2004 to 2006

7 Discussion

To be able to understand the results in this study we need to take a look at which reservoir changes that may have taken place and that may have affected the seismic data. We know that this is a producing hydrocarbon reservoir where water injectors are used to maintain the pressure in the field. We also know that the field were initially undersaturated and that production started in July 2000 without injectors as pressure support. What we also know is that the pressure in the segment got to low so a water injector had to be drilled downflank in the water zone of the G-segment to give pressure support and flush the hydrocarbons in the direction of the producer. This introduces a set of pressure and saturation variables that may have affected the seismic response from the field.

Interpretations done on mapping fluid fronts and pressure build up in the the Norne main field and in the surrounding fields is often done using direct interpretations of the fluid contacts and the movement of the contacts from one survey to another (e.g. Lygren et al. (2005); Osdal (2004); Ouair et al. (2005); Osdal et al. (2006); Alsos et al. (2009); Osdal and Alsos (2010)). In the result part of this thesis on the other hand, few seismic sections with direct interpretation of the fluid contacts has been shown. The reason for this is that the oil leg and reservoir interval in the G-segment is relatively thin and more than one 4D effect affects the seismic response at the same time. Different signs and rates of pore pressure variations, balancing pore pressure on a level around the bubble point of the hydrocarbons in the segment and water replacing oil in parts of the segment makes the interpretations challenging. Amplitude differences, pore pressure attributes and time shifts has been essential for the understanding of the production changes in this thesis.

To get a history of reservoir changes up to the time of the 2001 survey we can look at Osdal et al. (2006) interpretation of 4D impedance difference data on Top Garn Formation in the G-segment between the original seismic base-survey in 1992 and the first Q-marine survey in 2001. They showed that there was a decrease in acoustic impedance from 1992 to 2001 in the whole hydrocarbon bearing part of the G-segment, Figure 31. When production well 6608/10-E-4 started to produce oil the pore pressure depleted to a level of approximately 200 bar, which was below the bubble point for the hydrocarbons in the segment. As a result of this, gas were going out of solution, causing the drop in acoustic impedance in the segment. The drop in impedance outlined the whole hydrocarbon bearing part of the G-segment, Osdal et al. concluded then that there were no pressure barriers between the E-4 producer and the rest of the oil in the segment. An updated reservoir model for the

G-segment was made with this results as input.

In the Osdal et al. paper results of a rock physical analysis for the effect of fluid substitution, where gas is going back to oil, and the effect of different pore pressure in the Garn Formation were published. The model for the fluid substitution was calculated using Gassmann's equations, Equation 1, while the velocity versus pore pressure curve was derived from core plug measurements in the laboratory. An adjustment of the pressure versus velocity curve were performed after interpretation of 2001 to 2004 difference data. Figure 32 shows the rock physics results where the left plot gives the P-wave velocity versus pore pressure and the right plot shows P-wave velocity versus gas saturation.

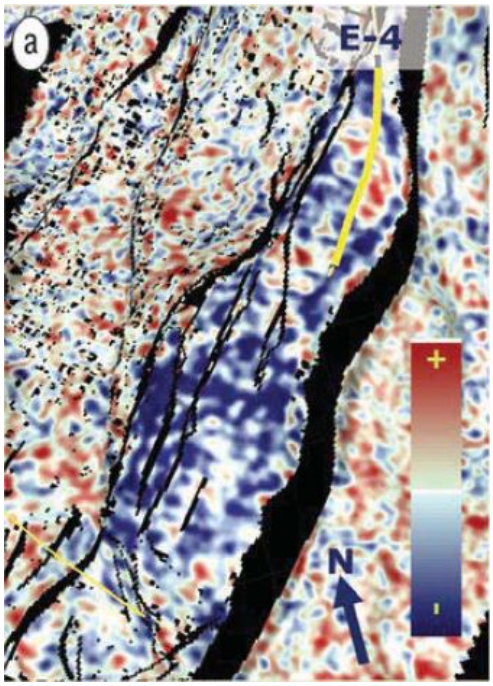

Figure 31: 4D impedance difference data between the 1992 and 2001 surveys. Blue is related to decreased impedance. After producer 6608/10-E-4 started to produce the pressure in the field dropped to below the bubble point of the hydrocarbons in place. Gas going out of solution caused the decrease in impedance. The fact that the anomaly is outlining the whole segment indicated that there were no pressure barriers between the E-4 producer and the rest of the oil in the segment. From (Osdal et al., 2006)

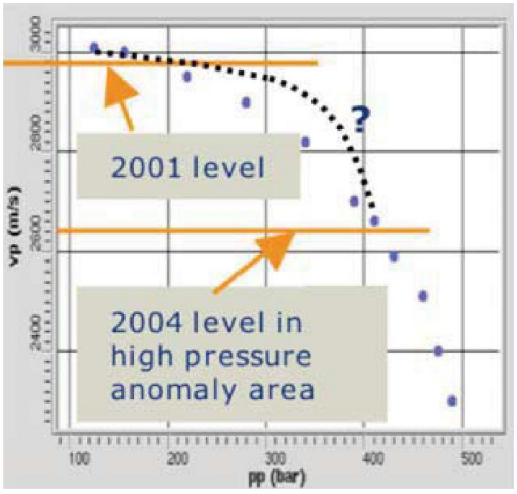

(a) P-wave velocity versus pore pressure

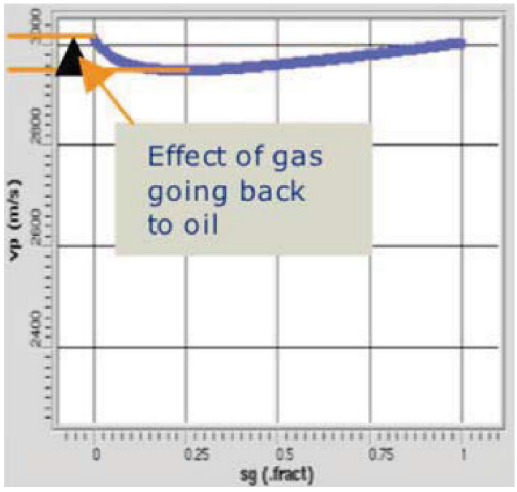

(b) P-wave velocity versus gas saturation

Figure 32: Rock physical analysis for the Garn formation. **a):** P-wave velocity versus pore pressure. Blue dots in shows velocity versus pore pressure curve derived from core plug measurements in the laboratory, black dots are updated velocity versus pressure curve fitted to field observations. **b):** P-wave velocity versus gas saturation derived using Gassmann's equations. From Osdal et al. (2006)

7.1 2001

With Osdal et al. (2006) interpretations in mind, we can look at the amplitude response of Top Garn Formation, top reservoir, in 2001, Figure 20. The variation in reflectivity on the Top Garn Formation indicates that some rock or fluid properties are changing along this horizon. By assuming that the rock framework does not change much the changes may be addressed to differences in the fluid saturation. Gassmann's equation, Equation 1, gives that the acoustic impedance in a porous rock will decrease with fluid substitution from water to more easily compressible oil or gas. This will on Top Garn Formation mean a more negative amplitude response in the hydrocarbon filled segments compared to the water filled segments along the horizon.

Figure 33(a) shows an intercept-gradient, R_0-G, cross-plot of the background trend for the lithologies in a water filled interval derived from a time window of 300 ms close to the reservoir at the Norne field, the position for the background trend is marked with purple circle in Figure 20. We can clearly see that the background trend is going from the second quadrant with negative intercept and positive gradient, through the origin of the R_0-G coordinate system and into the fourth quadrant with positive intercept and negative gradient. The red line is a trend line for the background lithologies. Figure 33(b) shows R_0-G cross-plot for the AVO-response on the Top Garn Formation in a high amplitude zone in the G-segment, yellow circle in Figure 20. We can clearly see that the points in the cross-plot is plotting away from the background trend with a more negative intercept and gradient than the background lithologies. In Figure 15 in we saw that saturation changes and pore pressure changes follows different trend lines in cross plots. The response in Figure 33(b) follows the fluid trend well and indicates that the high amplitudes of the G-segment contains a lighter fluid than water.

Correlation of the transition between high negative and less negative amplitudes on Top Garn Formation with the interpretation of the initial hydrocarbon contacts in the field, given in Statoil (1994), gives a good match, Figure 34. Also noting that the transition between high and low negative amplitudes lines up well with the time-contours on the Top Garn Formation let us make the statement that the changes in fluid properties causes most of the variation in amplitude along this horizon.

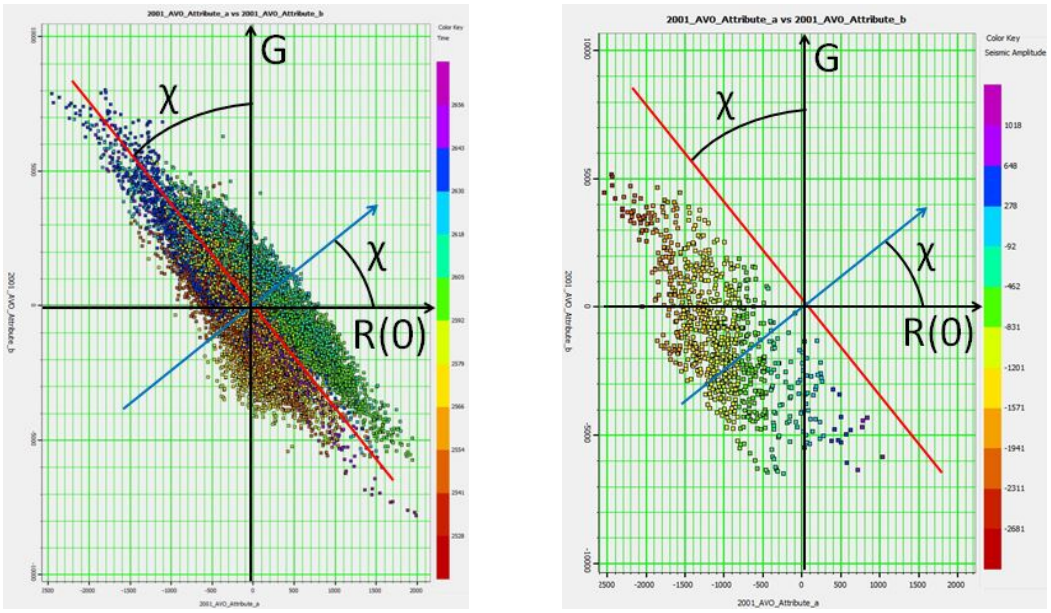

(a) R_0-G cross-plot of the background lithologies

(b) R_0-G cross-plot for the AVO-response on Top Garn Formation, G-segment

Figure 33: a): R_0-G cross-plot of the background trend for the lithologies in a water filled interval of 300 ms close to the reservoir at the Norne field. **b):** R_0-G cross-plot for the AVO-response on the Top Garn Formation in a high amplitude zone in the G-segment. We can clearly see that the points in the high amplitude zone in the G-segment plots away from the background trend indicating different fluids

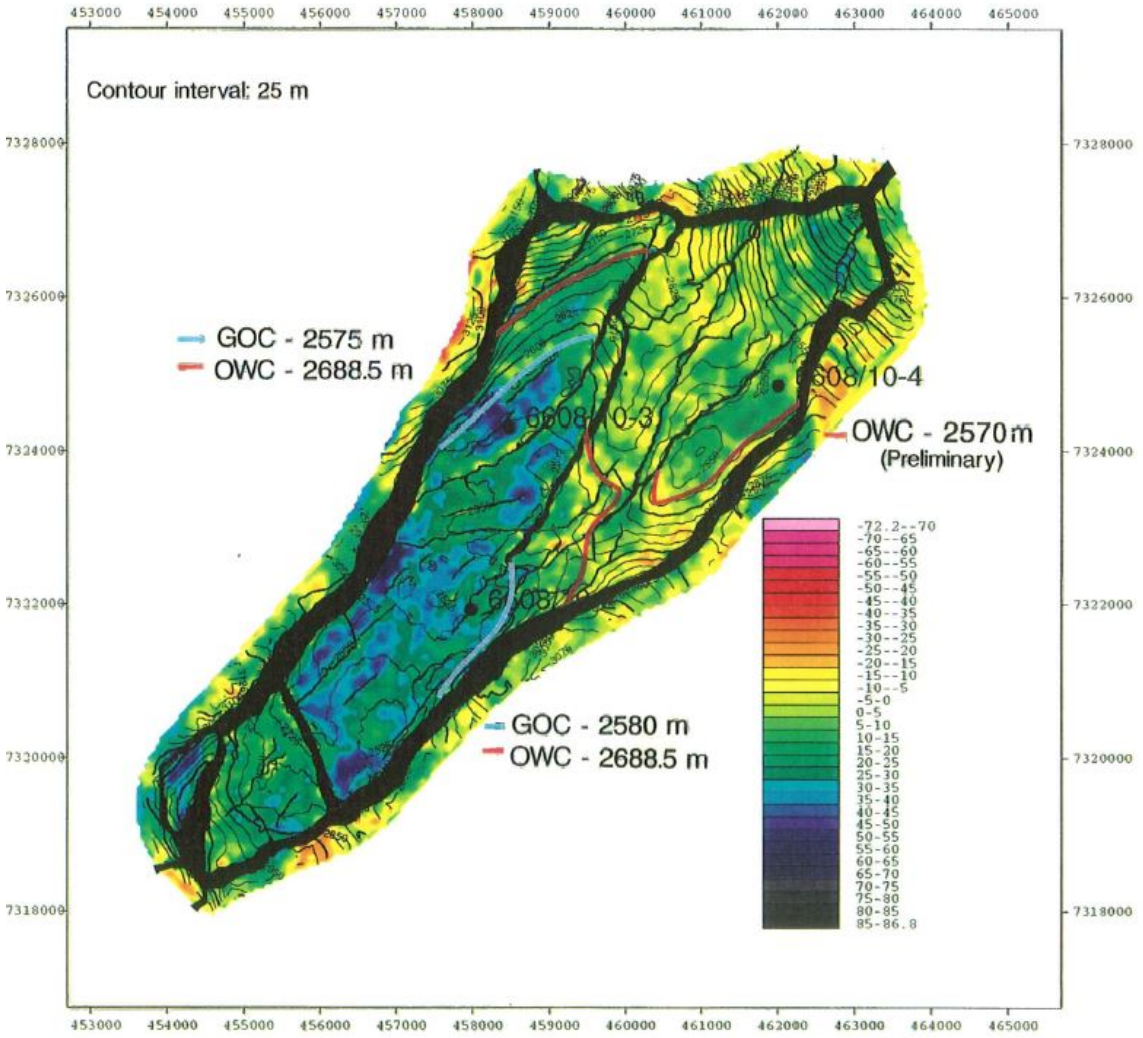

Figure 34: Top reservoir map showing owc and goc for the Norne field in 1994. Note the good correlation between the fluid contacts and the high amplitude zones of the Top Garn Formation in Figure 20. From Statoil (1994)

7.2 2003

The area covered by the negative amplitude difference anomaly around water injector 6608/10-F-4 and up along the western main fault between the 2001 and 2003 surveys correlates well with the anomalies for the increase in pore pressure-change attribute and the positive time shifts between the 2001 and 2003 surveys. This good correlation of attributes in combination with the knowledge that the injector was active from September 2001, Figure 9, all gives strong indications that the pore pressure rose between 2001 and 2003 and caused the anomalies seen in this part of the segment. From the theory part of this thesis it is given that an increase in pore pressure in the reservoir will weaken the pressurized rock framework and, according to Equation 12 and Equation 13, reduce both the P- and S-wave velocities. The reduction in seismic velocities will decrease the acoustic impedance, give a negative amplitude difference response and an increased pore pressure attribute on top of the pressurized zone. The seismic travel times for waves propagating through the pressurized rocks will increase and cause positive time shifts for reflectors below the reservoir. All in accordance with the observed anomalies.

The reset of the segment shows the opposite amplitude difference and an anomaly of decreased saturation-change attribute. No significant time shift and no detectable trend in the pore pressure-change attribute are seen in this area. The positive amplitude difference imply that the impedance, and hence the P-wave velocity must have increased in this part of the segment. This is also in accordance to the the decreased saturation-change attribute. An early interpretation may be that water has flooded this part of the segment and increased the incompressibility of the fluids. Because of no detected water production in production well 6608/10-E-4 between 2001 and 2003, Figure 9, this theory is unlikely to be valid. A more reasonable theory is that also the pore pressure in this part of the segment has increased after start of injection in 2001. The pore pressure increase has led to gas going back to oil, and hence increased the incompressibility of the fluids in the segment. Osdal et al. (2006) interpretation of the base to 2001 surveys showed that gas had gone out of solution also along the western main fault. It is likely that the gas has gone back to oil in this part of the segment too, but the effect of this has been overshadowed by the effect of the increased pore pressure. From the rock physical analysis given in Figure 32 we can see that the pore pressure increase must be significantly lower in the part of the G-segment with positive amplitude difference than along the western main fault. Otherwise, both anomalies would have shown the same sign on the amplitude difference map.

Figure 35(a) shows seismic cross-line 1940 from the 2003 survey, location of this line is marked yellow in Figure 21(a). The line shows a fault going through the reservoir zone in the G-segment. Figure 35(b) shows the 2001 to 2003 difference data for the same line. The difference data clearly shows that the fault is located exactly at the transition between the positive and the negative amplitude anomalies marked by yellow and blue circles. As discussed above, the pressure in the positive amplitude difference anomaly must be significantly lower than the pressure in the negative amplitude difference anomaly. This means that the fault identified in the cross-section works as a pressure barrier that is separating a high pore pressure build up along the western part of the G-segment from a more moderate pressure build up in the main part of the G-segment.

Figure 36(a) and Figure 36(b) shows seismic in-line 1237, Figure 21(a) for location, from the 2003 survey and the 2001 to 2003 difference data for the same line. The difference data shows how the anomaly changes sign, but in the 2003 data no fault or other barrier can be identified. The pressure barrier in this direction must be sub-seismic, below the resolution of the seismic data.

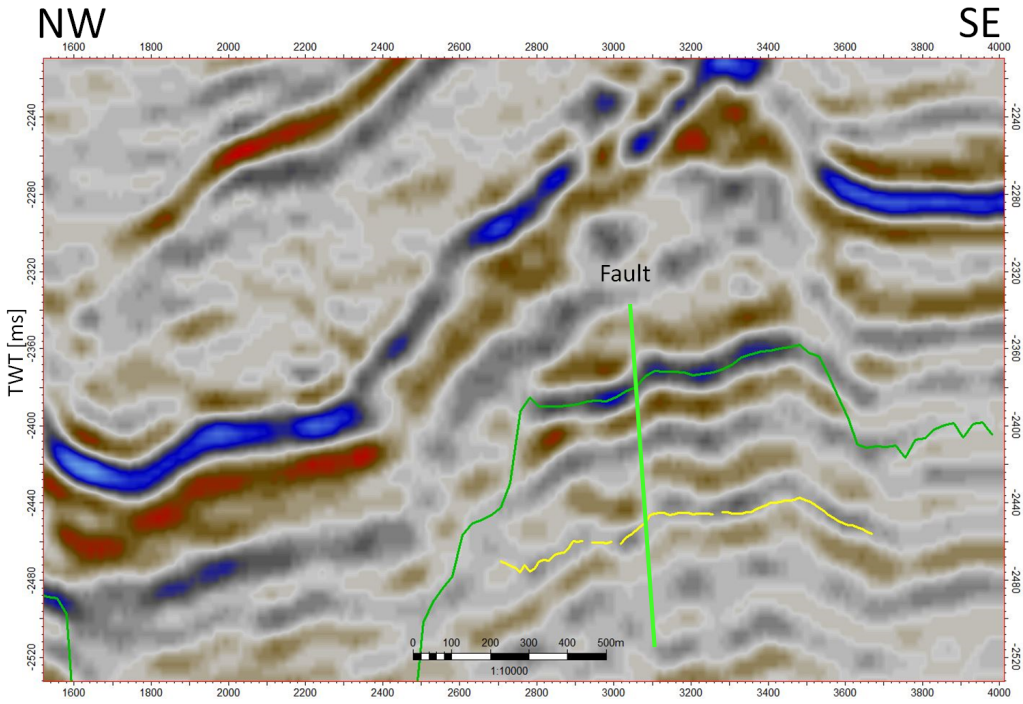

(a) Cross-line 1940, 2003

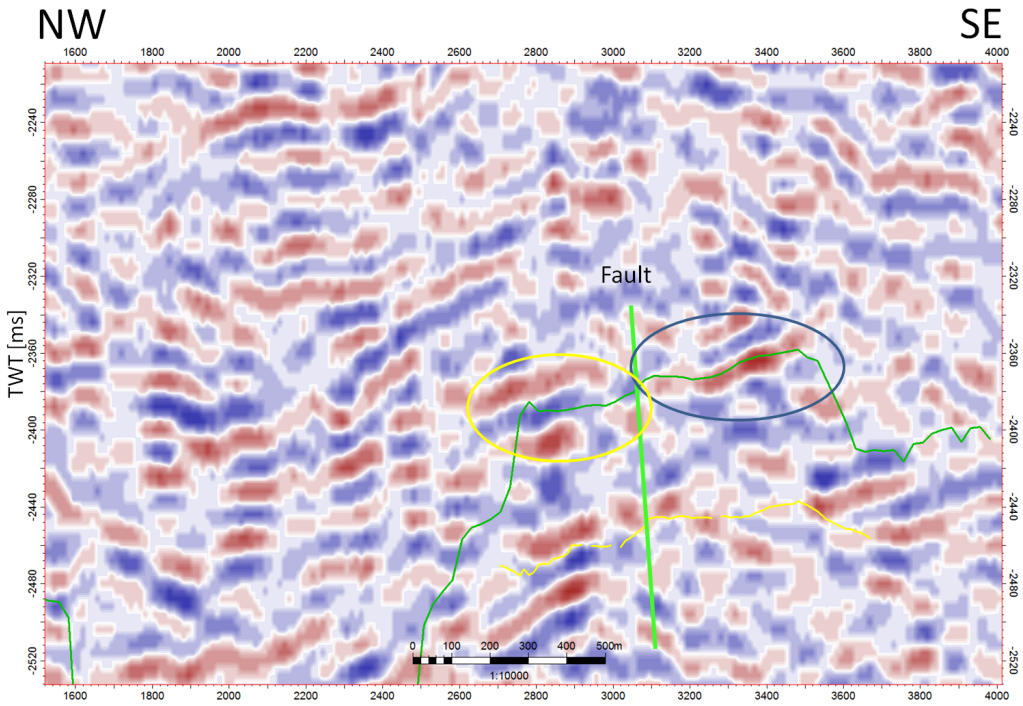

(b) Cross-line 1940, 4D 2001 to 2003

Figure 35: a): Seismic cross-line 1940, 2003 showing a fault going through the reservoir zone in the G-segment. **b):** Seismic cross-line 1940, 2001 to 2003 difference data. The fault marks the transition between the positive and negative amplitude difference anomalies marked by blue and yellow circles

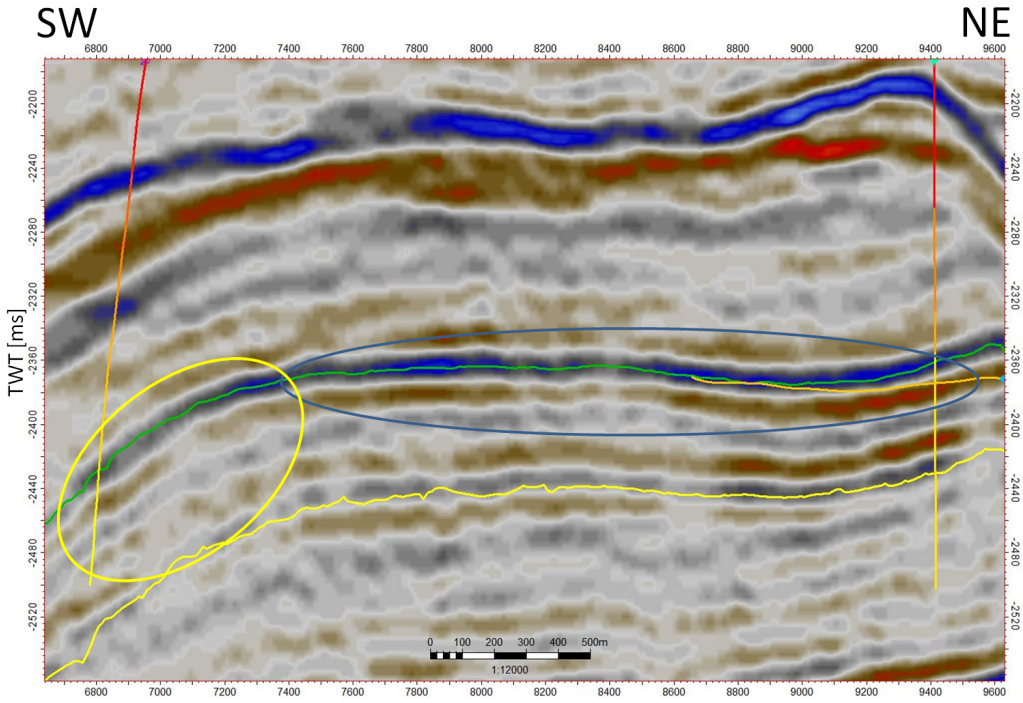

(a) In-line 1237, 2003

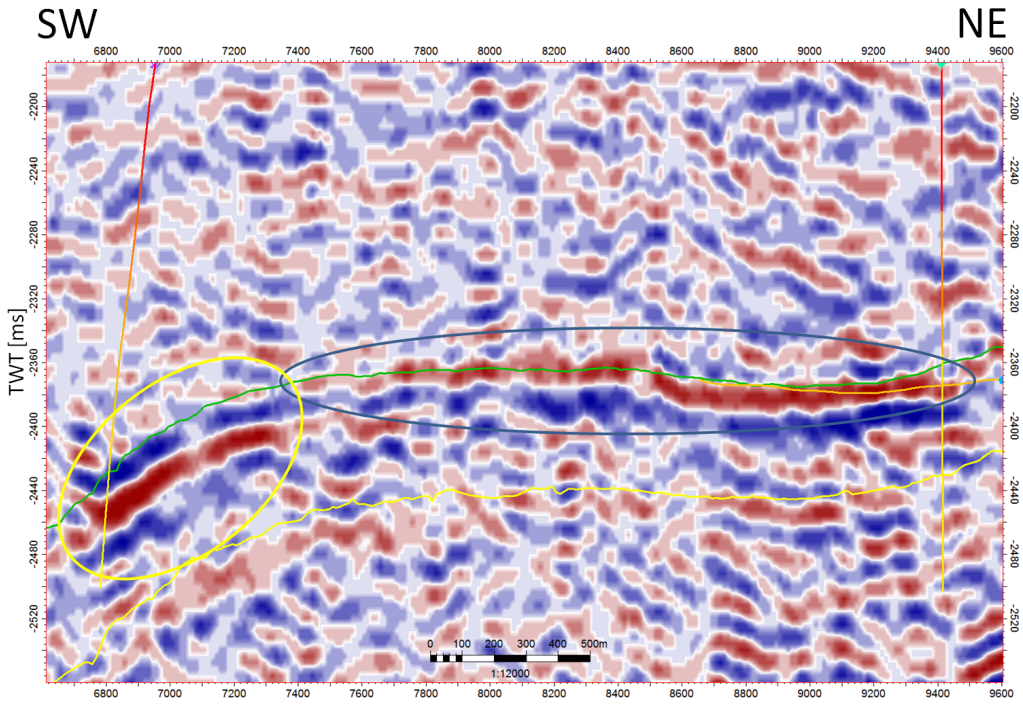

(b) In-line 1237, 4D 2001 to 2003

Figure 36: a): Seismic in-line 1237, 2003. No fault or other barriers can be identified in the area of the changing sign of amplitude difference observed in the 4D 2001 to 2003 difference data shown in b). **b):** 4D 2001 to 2003 difference data for the same in-line. Blue and yellow circles marks the position of the positive and negative amplitude difference anomalies

7.3 2004

The expand and growth of the negative amplitude difference, pore pressure-change attribute and time shift anomalies between 2003 and 2004 shows that the pore pressure was still increasing in the area around the injector and along the western main fault. A close examination of the amplitude difference map between the 2003 and 2004 surveys revealed an anomaly of positive amplitude difference around the toe of producer 6608/10-E-4. The anomaly is not identified on any of the other attribute maps. Figure 37(a) and Figure 37(b) shows seismic in-line 1227 in 2004 and the 2003 to 2004 difference data, respectively. Location of the in-line is marked yellow in Figure 23(b). The amplitude anomaly around the toe of the producer in the difference data has abrupt termination to south-west. By analysing the 2004 data a discontinuity of the seismic horizon below Top Garn Formation and a more dim amplitude response on Top Garn Formation is detected at the same position as the amplitude anomaly is terminating in the seismic difference section. A possible interpretation is a small fault located at this position. The fault can act as a minor pressure barrier that has limited the rate of pore pressure increase in the part of the G-segment limited by the positive amplitude difference on the 2003 to 2004 amplitude difference map. Because of the limited rate of pore pressure build up, dissolved gas were still in place in this part of the segment in 2003. After further increase in pore pressure between 2003 and 2004 the pore pressure exceeded the bubble point for the hydrocarbons and also the gas in this part of the segment went back to oil causing the more positive amplitude response between 2003 and 2004. The saturation-change attribute is to noisy to catch up this effect.

The negative amplitude difference response between the injector and the positive amplitude difference anomaly on the 2003 to 2004 amplitude difference map, in addition to an increased time shift and pore pressure-change attribute in the same area, gives strong indications that the pore pressure generally rose in the G-segment between 2003 and 2004.

The 2001 to 2004 time shift map does also contain positive time shift anomalies at and around the positions of the water injectors in the E-segment. The anomalies is strongest right at the position of the two injectors. This is a good indication that the effect of pore pressure increase caused by injectors is the largest contributor to the time shifts observed in this field.

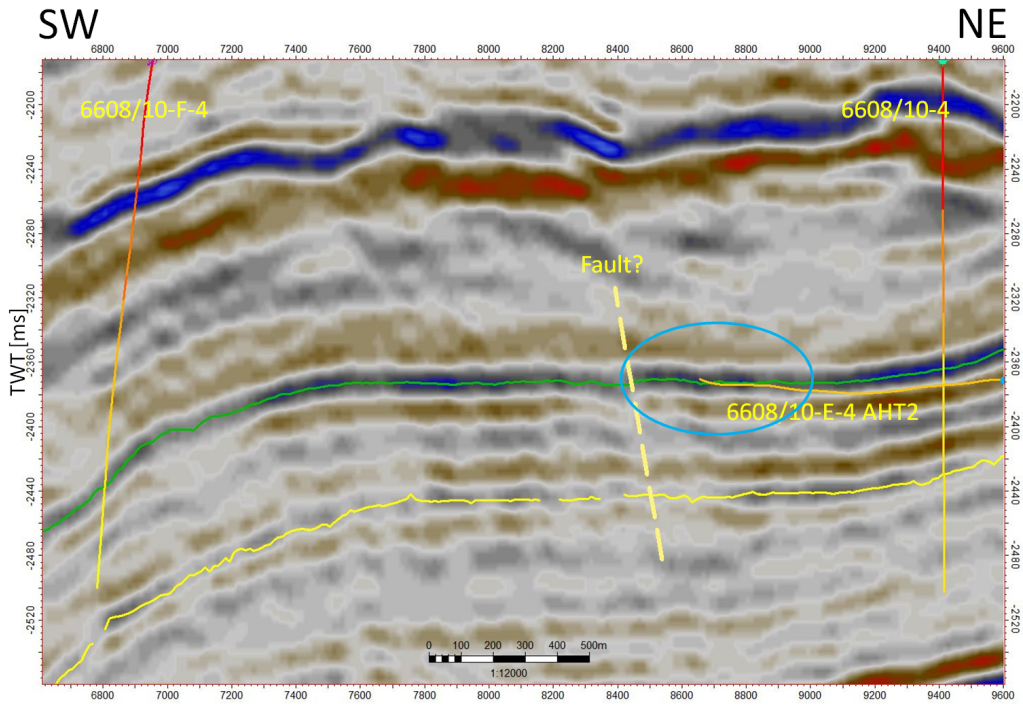

(a) In-line 1227, 2004

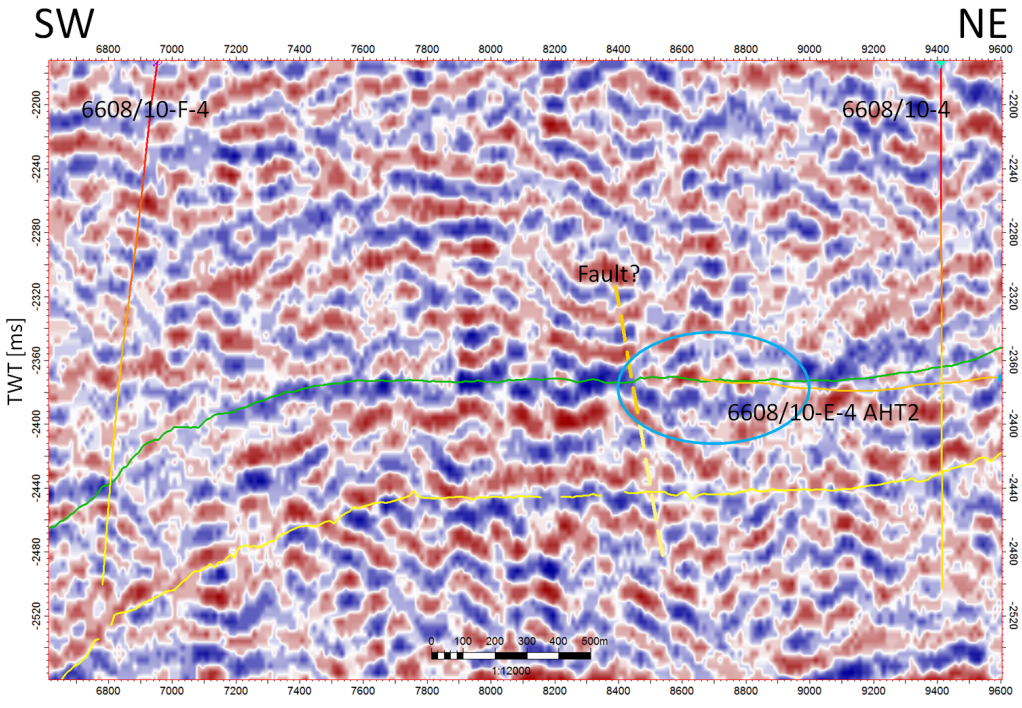

(b) In-line 1227, 4D 2003 to 2004

Figure 37: a): Seismic in-line 1227, 2004. A small fault can be identified at the position of the termination of the positive amplitude difference anomaly observed in b). **b):** 4D 2003 to 2004 difference data for the same line. Anomaly of positive amplitude difference marked by blue circle

7.4 2006

After the water production in producer 6608/10-E-4 got to high the well was shut in July 2005. Evidences of this can clearly be seen in the seismic difference data. A negative amplitude difference can be observed in the north-eastern part of the G-segment in the 2004 to 2006 amplitude difference map. Also the pore pressure-change attribute and time shift map shows the same anomaly. Up to 2005, while the producer was still active the pore pressure in the north-eastern part of the G-segment increased, but the rate of increase were limited by the extraction of hydrocarbons from the formation. The effect of gas going back to oil was the ruling effect on the 4D difference data. After the shut in of the well in 2005 the pore pressure in the north-eastern part of the segment had no producing well to limit the pressure build up and the pore pressure increased to a higher level. At the time of the 2006 survey the velocity decrease as a result of pore pressure increase had overprinted the effect of the gas going back to oil also in this part of the G-segment.

The 2001 to 2006 amplitude difference data shows that the negative amplitude difference anomaly is continuous all the way from injector 6608/10-F-4 along the western main fault and up to the north-eastern part of the G-segment. This is a clear indication that the connectivity between the pores is much better along the western part of the G-segment than from the injector and directly to the producer. The most probable path for water flooding is from the injector, along the western main fault through the area limited by the pressure barriers identified on the 2001 to 2003 data and into the north-eastern part of the G-segment and to the heal part of producer 6608/10-4. A production logging test (PLT) was performed in the producer in 2005. Unfortunately only the first half of the well was logged so no information from the toe of the well were collected. The test showed high water cut in the heal area of the producer which fits this 4D interpretations good.

7.5 Data quality

For the result and discussion part of this thesis several methods are used and correlated to best link the changes in seismic data to production changes in the field. The quality and sensitivity of the different methods are varying. The amplitude maps shows very good and firm results. The signal to noise level is relatively high making it possible to detect anomalies and define their boundaries on a detailed level. Comparing the time shift maps to the amplitude maps, only the negative amplitude difference anomalies are visible on the time shift maps. The reason for this is that the amplitude maps measure the differences directly on an interface between two layers. Small variations in rock properties in one of the layers, changes the contrast between the two layers and affects the amplitude of the seismic signal directly. The time shift analysis on the other hand, is an indirect way of measuring changes in properties. In time shift analysis one is measuring changes in velocities over an interval. The reservoir interval in the Norne G-segment is relatively thin, reservoir sands of 25 - 30 m and the oil leg approximately 15 meter (Statoil, 2004; NPD, 2013). From the results of the rock physics analysis, Figure 32, it is shown that the variation in P-wave velocity with varying saturation is maximum 70 m/s. This gives a time shift of maximum 0.2 ms through the oil column in the G-segment, far bellow the sensitivity of the time shift map. In addition, the fluid substitution where gas is going back to oil is driven by increased pore pressure, which tend to give time shift in the opposite direction. In this study, sensitivity for time shifts is around 1 ms.

Although the effect of saturation changes are not visible on the time shift data, the effect of increased pore pressure is detectable and well pronounced. A reason for this is that the pore pressure increase can give velocity changes of higher degree than the saturation changes and the effect can take place in the whole reservoir segment, not only the oil leg. Observed time shifts on the difference data in this thesis is up to 3.5 ms, which correspond to a velocity decrease of approximately 600 m/s.

Though, the pore pressure-change and saturation-change attribute maps contains a high level of noise relatively good results are obtained on the pore pressure-change attribute maps, but the saturation-change attribute maps shows some varying results. The saturation-change attribute maps does not detect all the expected changes. Specially, the supposed water flooding in the area along the western main fault is not detected on any of the maps. The reason for the noise and poor results may be more than one: Firstly, the assumptions made when linking the rock physics analysis to the changes in seismic velocities may be questioned. The laboratory measurements

and rock physics modelling may not reflect the real field situation and assuming that the modelled results are valid for the whole segment may be wrong. Secondly, the seismic repeatability between the different surveys may be to low, making it hard to detect small changes. Thirdly, scaling factors used in the near-, mid- and far-stack cubes may be questioned. This can cause noisy attribute map and cause leakage from attribute map and into the other. Moreover, by investigating the vectors for the saturation-change attribute and the pore pressure-change attribute one can show that the two vectors are not perpendicular to each other. This means that a significant change in the pore pressure-change attribute do also add a component to the saturation change attribute, even though the saturation does not change. The pore pressure increase along the western main fault is assumed to be significant, so the effect of increased pore pressure may have overprinted the effect of saturation changes along the fault.

An effect that has not been discussed in this thesis is the effect of tuning. Both the amplitude maps and the AVO results may have been affected by this. Tuning can occur when seismic reflectors are closely spaced, like the top and base reservoir in the Norne G-segment. Tuning causes interference in the seismic signal. The effect is dependent on the spacing between the reflectors and the frequency of the seismic pulse.

8 Conclusion

In this thesis interpretation of pressure and saturation changes in the Norne G-segment have been performed for the time interval between 2001 and 2006. By use of amplitude difference maps and AVO attribute maps for the seismic horizon representing top of the reservoir in addition to time shift maps for a seismic horizon below the reservoir the pressure and saturation history has been revealed.

Due to a relatively thin reservoir interval and the fact that more than one 4D effect has affected the seismic response at the same time, direct interpretation of the oil-water contact and the movement of the contact from one seismic survey to another has not been possible to do on the dataset used in this thesis.

Pore pressure increase, pore pressure decrease, gas going back to oil and water flooding oil are effects that have changed the rock parameters in the G-segment.

The following points can summarize the results in this thesis:

- The pore pressure build up caused by injector 6608/10-F-4 has led to a generally increase in pore pressure in the whole G-segment after start of injection in September 2001.
- The pressure increase between 2001 and 2003 led to gas going back to oil in the major part of the segment.
- The pore pressure increased more around the injector and in the area along the western main fault than in the rest of the segment between 2001 and 2004.
- A fault parallel to the western main fault has acted as a pressure barrier and separated a build up of high pore pressure along the western main fault from a more gentle pressure build up in the main part of the field. No pressure barrier in the south-east to north-east direction has been detected on any of the seismic surveys, but due to different signs on the amplitude difference anomalies a sub seismic pressure barrier must be in place and limit the pressure build up also in this direction.
- A small area has been identified around the toe of producer 6608/10-E-4 where the rate of pore pressure increase was lower than in the rest of the segment. The gas out of solution in this compartment did not go back to oil before after the seismic acquisition in 2003.
- After the shut in of producer 6608/10-E-4 in July 2005 the pressure in the

north-eastern part of the segment increased significantly.

- Expected flow path for water flooding the G-segment has been identified to be from the injector, along the western main fault through the area limited by the pressure barriers mentioned above and into the north eastern part of the G-segment to the heal of producer 6608/10-E-4.

For further work I will recommend to model the effect of seismic tuning both on the amplitude difference data and on the AVO data. Because of the thin reservoir segment and oil leg tuning is assumed to give interference between the top and base horizon in the segment. The result of this study can also be implemented in a simulation software to see if the flow and pressure build up in the simulation model would match the interpreted 4D changes and to predict the results of further production.

References

Alsos, T., B. Osdal, and A. Høiås (2009). The many faces of pressure changes in 4d seismic at the svale field and its implication on reservoir management. *71st EAGE Conference & Exhibition, Amsterdam, Netherlands 8-11 June*.

Arre, V. (2007). Estimating 4d velocity changes and contact movement on the norne field. *Offshore Technology Conference, Huston, Texas 30 April-3 May*.

Avseth, P. (2011). Explorational rock physics - the link between geological processes and geophysical observables. In *Petroleum Geoscience: From Sedimentary Enciroments to Rock Physics*. Springer-Verlag Berlin Heidelberg.

Avseth, P., T. Mukerji, and G. Mavko (2005). *Quantitative Seismic Interpretation - Applying Rock Physics Tools to Reduce Interpretation Risk*. Cambridge University Press, Cambridge, UK.

Domenico, S. N. (1976). Effect of brine-gas mixture on velocity in an unconsolidated sand reservoir. *Geophysics 41 (5)*, 882–894.

Gassmann, F. (1951). Elastic waves through a packing of spheres. *Geophysics 16*, 673–685.

Gjerde, J., D. Tuppen, and P. Skillingstad (2002). Geological and petrophysical report norne field pl 128 well 6608/10-f-4h. Technical report, Statoil.

Gjerstad, H. M., I. Steffensen, and J. I. Skagen (1995). The norne field - exploration history & reservoir development strategy. *Offshore Technology Conference, Huston, Texas 1-4 May*.

Greaves, R. J. and T. J. Fulp (1987). Three-dimensional seismic monitoring of an enhanced oil recovery process. *Geophysics 52 (9)*, 1175–1187.

Hatchell, P. and S. Bourne (2005). Rocks under strain: Strain-induced time-lapse time shifts are observed for depleting reservoirs. *The Leading Edge 24 (12)*, 1222–1225.

Landrø, M. (1999). Repeatability issues of 3-d vsp data. *Geophysics 64 (11)*, 1673–1679.

Landrø, M. (2001). Discrimination between pressure and fluid saturation changes from time-lapse seismic data. *Geophysics 66*, 836–844.

Landrø, M. (2008). Anvendt geofysikk i tpg4100 fysikk og geofysikk.

Landrø, M. (2011). 4d seismic. In *Petroleum Geoscience: From Sedimentary Enciroments to Rock Physics*. Springer-Verlag Berlin Heidelberg.

Lygren, M., O. Husby, B. Osdal, Y. E. Ouair, and M. Springer (2005). History matching using 4d seismic and pressure data on the norne field. *EAGE 67th Conference & Exhibition, Madrid, Spain 13-16 June*.

Mavko, G., T. Mukerji, and J. Dvorkin (2009). *The Rock Physics Handbook; Tools for Seismic Analysis of Porous Media*. Cambridge University Press, New York.

Mavko, G. and A. Nur (1975). Melt squirt in the asthenosphere. *Journal of Geophysical Research 80*, 1444–1448.

Mindlin, R. D. (1949). Compliance of elastic bodies in contact. *J. Appl. Mech. 16*, 259–268.

NPD (2013). *Norwegian Petroleum Directorate's FactPages*. [Online] June 2013. Available from: `http://factpages.npd.no/factpages/`. [Accessed: 17th June 2013].

Nur, A., C. Tosaya, and D. Vo-Thanh (1984). Seismic monitoring of thermal enhanced oil recovery processes. *SEG Technical Program Expanded Abstracts*, 337–340.

Osdal, B. (2004). Using high quality and repeatable q-marine data in reservoir monitoring on the norne field. *EAGE 66th Conference & Exhibition, Paris, France 7-10 June*.

Osdal, B. and T. Alsos (2010). Norne 4d and reservoir management - the keys to success. *72nd EAGE Conference & Exhibition incorporating SPE EUROPEC 2010, Barcelona, Spain, 14 - 17 June*.

Osdal, B., O. Husby, H. A. Aronsen, N. Chen, and T. Alsos (2006). Mapping the fluid front and pressure buildup using 4d data on norne field. *The Leading Edge 25(9)*, 1134–1141.

Ostrander, W. J. (1984). Plane-wave reflection coefficients for gas sands at nonnormal angles of incidence. *Geophysics 49*, 1637–1648.

Ouair, Y. E., M. Lygren, B. Osdal, O. Husby, and M. Springer (2005). Integrated reservoir management approach: From time-lapse acquisition to reservoir model update at the norne field. *International Petroleum Technology Conference, Doha, Quatar 21-23 November*.

Sava, D., T. Mukerji, M. Diaz, and G. Mavko (2000). Seismic detection of pore fluids: Pitfalls of ignoring anisotropy. *SEG Annual Meeting August 6-11 Calgary, Alberta*.

Shuey, R. T. (1985). A simplification of the zoeppritz equations. *Geophysics 50 (4)*, 609.

Smith, G. C. and P. M. Gidlow (1987). Weighted stacking for rock property estimation and detection of gas. *Geophysical Prospecting 35*, 993–1014.

Statoil (1994). Norne field - plan for development and operation. support documentation 1: Reservoir geology.

Statoil (2001a). Geological and petrophysical report norne field pl 128 wells 6608/10-e-4 h, 6608/10-e-4 t2 h, 6608/10-e-4 ah, 6608/10-e-4 a t2 h. Technical report, Statoil.

Statoil (2001b). Pl 128 norne reservoir management plan norne field.

Statoil (2004). Annual reservoir development plan norne field 2004.

Statoil (2006). Production and injection history to 2006. *Excell document from the Norne Full Field Database hosted by the IO Center at NTNU*.

WesternGeco (2007). Data processing report for statoil block 6608/10 (norne) st0113, st0103, st0305, st0409, st0603 2006 4d processing.

Zoeppritz, K. (1919). Erdbebenwellen vii. viib. *Über* reflexion und durchgang seismischer wellen durch unstetigkeitsflächen. nachrichten von der königlichen gesellschaft der wissenschaften zu göttingen. *Mathematisch-physikalische Klasse*, 66–84.